iScience

CellPress
OPEN ACCESS

Article

N^6-methyladenosine-modified VGLL1 promotes ovarian cancer metastasis through high-mobility group AT-hook 1/Wnt/β-catenin signaling

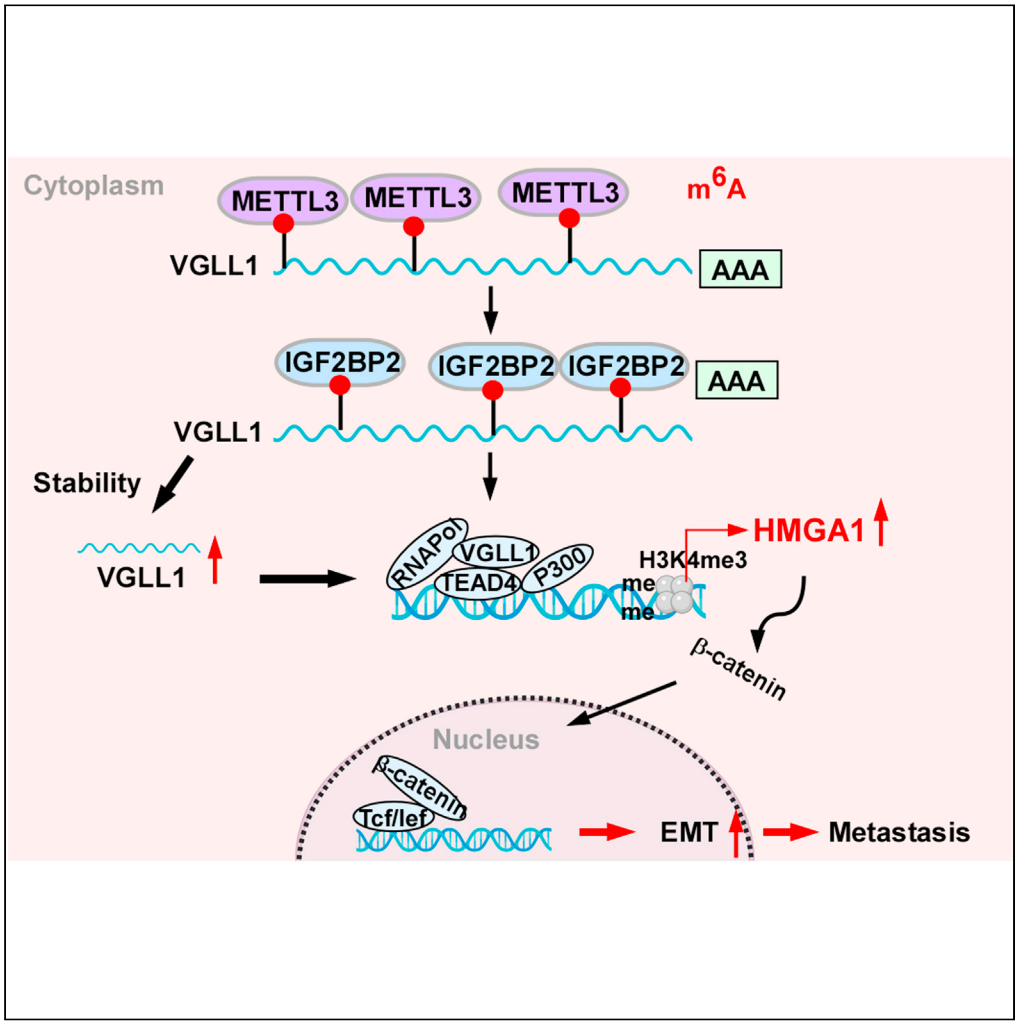

Han Li, Liming Cai, Qiuzhong Pan, ..., Yanna Zhang, Zhongqiu Liu, Jianchuan Xia

liuzq@gzucm.edu.cn (Z.L.)
xiajch@mail.sysu.edu.cn (J.X.)

Highlights

High expression of VGLL1 in ovarian cancer predicts poor prognosis

VGLL1 promotes ovarian cancer metastasis through HMGA1/Wnt/β-catenin signaling

HMGA1 is essential for VGLL1-mediated metastasis in ovarian cancer

VGLL1 inhibition offers new ideas for ovarian cancer treatment

Li et al., iScience 27, 109245
March 15, 2024 © 2024
https://doi.org/10.1016/j.isci.2024.109245

iScience

CellPress
OPEN ACCESS

Article

N^6-methyladenosine-modified VGLL1 promotes ovarian cancer metastasis through high-mobility group AT-hook 1/Wnt/β-catenin signaling

Han Li,[1,3,4] Liming Cai,[2,4] Qiuzhong Pan,[1,4] Xingyu Jiang,[1] Jingjing Zhao,[1] Tong Xiang,[1] Yan Tang,[1] Qijing Wang,[1] Jia He,[1] Desheng Weng,[1] Yanna Zhang,[1] Zhongqiu Liu,[2,*] and Jianchuan Xia[1,5,*]

SUMMARY

The main causes of death in patients with ovarian cancer (OC) are invasive lesions and the spread of metastasis. The present study aimed to explore the mechanisms that might promote OC metastasis. Here, we identified that VGLL1 expression was remarkably increased in metastatic OC samples. The role of VGLL1 in OC metastasis and tumor growth was examined by cell function assays and mouse models. Mechanistically level, METTL3-mediated N^6-methyladenosine (m^6A) modification contributed to *VGLL1* upregulation in an IGF2BP2 recognition-dependent manner. Furthermore, VGLL1 directly interacts with TEAD4 and co-transcriptionally activates HMGA1. HMGA1 further activates Wnt/β-catenin signaling to enhance OC metastasis by promoting the epithelial-mesenchyme transition traits. Rescue assays indicated that the upregulation of HMGA1 was essential for *VGLL1*-induced metastasis. Collectively, these findings showed that the m^6A-induced *VGLL1*/HMGA1/β-catenin axis might play a vital role in OC metastasis and tumor growth. *VGLL1* might serve as a prognostic marker and therapeutic target against the metastasis of OC.

INTRODUCTION

Ovarian cancer (OC) is the fifth most frequent cause of cancer-related death in women worldwide and is also the most fatal gynecological malignancy among female reproductive system cancers.[1] The broadly recognized feature of OC is abdominal cavity seeding, a form of dissemination in which cancer cells shed from tumors, circulate via the peritoneal fluid, and finally implant on the peritoneal and intestinal surfaces.[2] More than 70% of patients with OC are diagnosed at a disseminated stage, especially with the colonization of the peritoneum and intestines.[3] Despite advances in debulking surgery, chemotherapy regimens, targeted therapies, and immunotherapy, the 5-year survival rate of women with widespread peritoneal metastasis is less than 45%.[4] Tumor metastasis, especially peritoneal metastasis, is the most prominent clinical obstacle to the treatment of OC.[3] However, the exact mechanisms in OC metastasis remain unclear. Further research focusing on the mechanisms and key molecules involved in the process of metastasis is necessary to design therapeutic strategies with the potential to control OC progression.

The biological metastatic behavior of OC is unique, differing significantly from the classic hematogenous or lymphatic vasculature metastases in most other types of cancer[5]: OC cells disseminate predominantly into the peritoneal cavity from the primary tumor, where they implant on the abdominal surfaces and organs, especially the fallopian tubes, uterus, and intestines.[6] In addition, peritoneal cavity metastasis frequently correlates with the formation of malignant ascites, which in turn further facilitates OC cell metastasis.[7] As such, malignant ascites formation and peritoneal cavity implantation are key steps in OC metastasis, ultimately contributing to recurrence.[8]

Tumor relapse, mainly caused by tumor metastasis, is the major factor influencing the high mortality of patients with OC.[7] Recently, several studies have indicated that epithelial–mesenchymal transition (EMT) is one of the key factors that promotes cancer metastasis.[9] During EMT, epithelial markers containing E-cadherin and cytokeratins decrease, whereas mesenchymal markers, such as N-cadherin and Vimentin, increase.[10] Abnormal activation of the EMT process allows primary epithelial cancer cells to obtain strong mesenchymal properties, such as metastasis and chemoresistance, eventually leading to tumor cell survival in the circulatory system and subsequent colonization of distant organs.[11,12] Additionally, the EMT process is controlled by sophisticated signaling networks including the Wnt, Notch, and Hedgehog pathways.[13,14] Of these, Wnt/β-catenin signaling plays an important role in the development and promotion of the EMT process and tumor metastasis.[15] Therefore, EMT-based therapeutic intervention via the regulation of Wnt/β-catenin signaling activity is regarded as a promising strategy for treating OC metastasis.

[1]Sun Yat-sen University Cancer Center; State Key Laboratory of Oncology in South China, Collaborative Innovation Center for Cancer Medicine, Guangzhou 510060, China
[2]International Institute for Translational Chinese Medicine, Guangzhou University of Chinese Medicine, Guangzhou 510006, Guangdong, China
[3]Department of Gynecology, Guangdong Provincial People's Hospital, Guangdong Academy of Medical Sciences, Guangzhou, Guangdong, China
[4]These authors contributed equally
[5]Lead contact
*Correspondence: liuzq@gzucm.edu.cn (Z.L.), xiajch@mail.sysu.edu.cn (J.X.)
https://doi.org/10.1016/j.isci.2024.109245

Here, by performing RNA-sequencing analysis, we identified that the *VGLL1* is significantly elevated in OC tissues, especially in metastasis+ OC tissues. The *VGLL* family, named *VGLL1–4*, interacts with TEA domain transcription factors (TEADs) via their Tondu (TDU) domain and participates in cancer genesis and metastasis.[16–18] Recently, *VGLL1* was found to be upregulated in gastric cancer, malignant myoepithelial tumors, and triple-negative basal-like phenotype breast cancer.[19–21] Highly expressed VGLL1 interacts with TEADs to form a VGLL1-TEAD complex and then transcriptionally upregulates *MMP9* to enhance the proliferation and metastasis of gastric cancer cells.[20] These studies suggest that *VGLL1* might be an oncogenic protein that mediates tumor metastasis. However, the mechanism by which *VGLL1* regulates OC cell metastasis remains unclear.

Cancer cells undergo genetic and epigenetic changes to obtain metastatic properties.[22] Among these modifications, the N^6-methyladenosine (m^6A) modification is frequently found in mRNA and affects the fate of RNA in various ways, such as RNA splicing, nuclear export, translation, and RNA stability.[23] M^6A RNA methylation is catalyzed by m^6A WERs (termed "writers," such as METTL3, METTL14, and WTAP; "erasers," such as FTO and ALKBH5; and "readers," such as YTHDC1, YTHDC2, YTHDF1, YTHDF2, YTHDF3, and HNRNPC.[23] Among these methyltransferases, METTL3 is the key catalytic subunit. Readers specifically identify the m^6A modification and determine the fate of m^6A-modified mRNAs.[24] Studies have shown that m^6A modification is involved in diverse processes, such as tissue development, cancer metastasis and proliferation, and stem cell self-renewal.[25] Moreover, dysregulation of m^6A modification correlates markedly with the progression of several cancers, including OC, lung cancer, and colorectal cancer.[23,26,27] Nevertheless, the function of m^6A-modified mRNA in OC metastasis and its underlying mechanism are still unclear.

Herein, *VGLL1* expression was observed to be upregulated significantly in OC, especially in metastatic OC, and was associated with poor survival of patients with OC.

Knockdown of *VGLL1* significantly suppressed the proliferation, invasion, and metastasis of OC cells *in vitro* and peritoneal cavity metastasis *in vivo*. Mechanistically, *VGLL1* is m^6A-modified by METTL3, resulting in the upregulation of *VGLL1* in an insulin-like growth factor 2 mRNA binding protein 2 (IGF2BP2)-dependent manner. VGLL1 then interacts with TEAD4 to transcriptionally activate high-mobility group AT-hook 1 (HMGA1)/Wnt/β-catenin signaling. We confirmed the important role of the m^6A/VGLL1/HMGA1 axis in OC. Our findings indicated that *VGLL1* could be an important biomarker for metastasis prediction in OC, which suggests a valuable therapeutic strategy for OC by targeting VGLL1.

RESULTS

VGLL1 is upregulated in metastatic ovarian cancer tissues and is related to poor prognosis

To explore critical metastasis-related genes in OC, RNA-seq was carried out on five primary OC tissues and five paired metastatic OC nodules. The results showed a total of 30 mRNAs that were significantly altered with $Log_2^{Flod\ change\ (FC)}$ values > 2 and p value < 0.05 in metastatic OC nodules compared to primary OC tissues (Figure 1A). VGLL1 was remarkably upregulated in metastatic OC nodule OC tissues compared to primary OC tissues among the 30 mRNAs (Figure 1A). Notably, upon qRT−PCR validation in a larger cohort comprising 72 normal ovary tissues and 126 OC tissues, we found that *VGLL1* was markedly overexpressed in OC tissues (Figure 1B). Additionally, we used the GEPIA 2 tool[28] to analyze The Cancer Genome Atlas (TCGA) data and showed that *VGLL1* was remarkably upregulated in various types of cancers, including bladder carcinoma, cervical carcinoma, ovarian carcinoma, pancreatic adenocarcinoma, uterine corpus endometrial carcinoma, and uterine carcinosarcoma (Figure S1A), and correlated positively with poor prognosis in OC (Figures S1B and S1C).

Moreover, statistical analysis showed that the *VGLL1* expression level correlated markedly with metastasis status (Figure 1C) in a large cohort of patients with OC. Further analysis using qRT−PCR demonstrated upregulated *VGLL1* expression in metastatic tumor cells in peritoneal metastatic nodules compared with paired primary tumors, suggesting that VGLL1 is an important factor in promoting OC metastasis (Figure 1D).

Next, we evaluated the clinical significance of VGLL1 expression in 157 OC samples (Table S1), and we found that VGLL1 expression was remarkably correlated with FIGO stage ($p < 0.001$), intraperitoneal metastasis ($p = 0.027$), ascites with tumor cells ($p = 0.006$), vital status ($p < 0.001$) and tumor recurrence ($p = 0.001$) (Table S2). However, it was not detected or was marginally detected in normal ovary epithelial tissues and primary OC tissues without metastasis (Figure 1E). Moreover, VGLL1 levels were elevated significantly in OC cell lines compared with those in a normal human ovary epithelial cell line (HoSepiC) or the immortalized fallopian tube cell line (FT282) at both the mRNA and protein levels, as measured by qRT-PCR and western blotting (Figures S1D–S1F). Consistently, VGLL1 expression was higher in primary OC tissues than in normal ovary epithelial tissues (Figure S1G). Additionally, we detected the expression of VGLL1 in OC samples of different stages and found that it was a stage-specific expression in patients with OC (Figure S1H). Importantly, VGLL1 expression was higher in metastasis-positive OC tissues than in metastasis-negative OC tissues (Figure 1F). Correlation analysis revealed that a high VGLL1 level correlated markedly with patient vital status and metastatic status (Figure 1G).

Importantly, in patients with OC with high VGLL1 expression, metastasis occurred earlier, and their survival time was shorter (Figures 1H and 1I). Furthermore, multivariate Cox regression analysis showed that VGLL1 expression was an independent prognostic factor, along with intraperitoneal metastasis and tumor recurrence, for a worse prognosis in OC (Table S3).

Inhibition of VGLL1 suppresses ovarian cancer cell proliferation and metastasis *in vitro*

To further investigate the role of VGLL1 in the malignant phenotypes of OC, we established OC cell lines (A2780 and OVCAR3 cells) that were stably silenced or overexpressed *VGLL1* (Figures S2A and S2B).

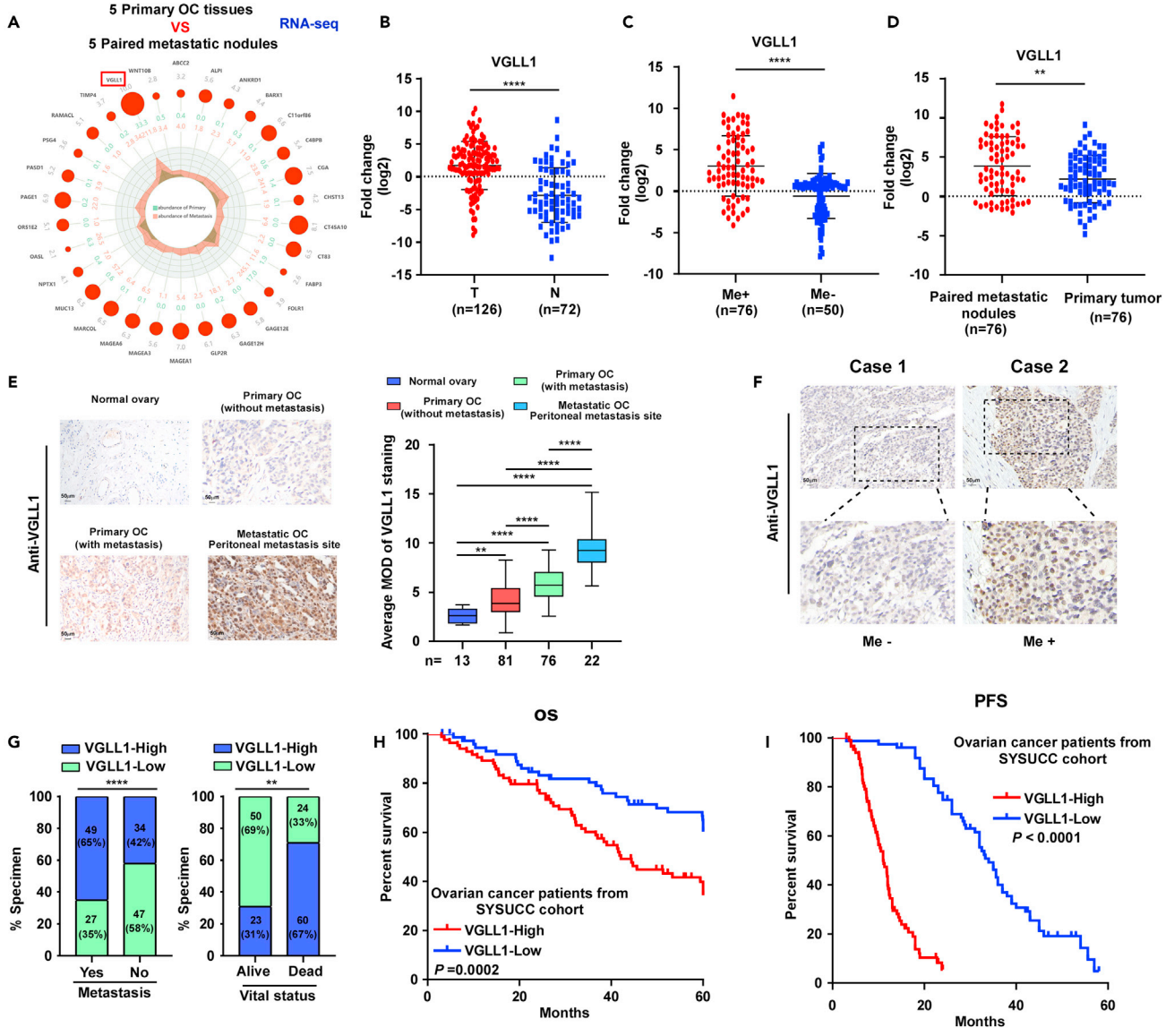

Figure 1. VGLL1 is upregulated in ovarian cancer tissues with metastasis and related to poor prognosis

(A) RNA sequencing of five primary OC tissues and five paired metastatic OC nodules to screen differentially expressed mRNA. Radar chart showing dysregulated 30 mRNA in primary OC tissues and paired metastatic OC nodules.

(B) qRT-PCR analysis of *VGLL1* expression in a 126 cases cohort of freshly collected human OC samples and a 72 cases cohort of freshly collected human normal ovary tissues.

(C) Comparison of *VGLL1* expression in Me+ and Me-ovarian cancer tissues.

(D) Comparison of *VGLL1* expression in primary human OC tissues and paired metastatic nodules.

(E) Immunohistochemistry analysis (left) and quantification (right) of VGLL1 expression in 13 normal ovarian tissues and 157 OC tissues, consist of 81 non-metastasis and 76 metastasis, and 22 metastatic OC nodules tissues (at peritoneal metastasis site), Scale bar, 50 μm (F). Representative IHC staining images of VGLL1 in OC tissues from 81 non-metastasis and 76 metastasis patients, Scale bar, 50 μm.

(G) VGLL1 strongly correlated with the status of tumor metastasis and patient survival. χ^2 statistical test was used. (H). Overall survival (OS) analysis in patients with OC stratified by low and high VGLL1 expression (n = 157, Kaplan-Meier method, log rank test).

(I) Progress-free survival (PFS) analysis in patients with OC stratified by low and high VGLL1 expression (n = 157, Kaplan-Meier method, log rank test). Me-: without metastasis; Me+: with metastasis. Student's t tests were used for comparing two variables. **p < 0.01, ***p < 0.001, ****p < 0.0001, ns indicates no significance. Each error bar represents the mean ± SD of three independent experiments.

We evaluated the function of VGLL1 in OC cell metastatic behavior. Wound healing and transwell assays showed that *VGLL1* silencing markedly inhibited the migration and invasion ability of OC cells, while VGLL1 overexpression had the opposite effect (Figures 2A, S2B–S2E, and S2G–S2L). Next, we detected the expression of EMT-related genes in VGLL1-knockdown or VGLL1-overexpressing OC cells and

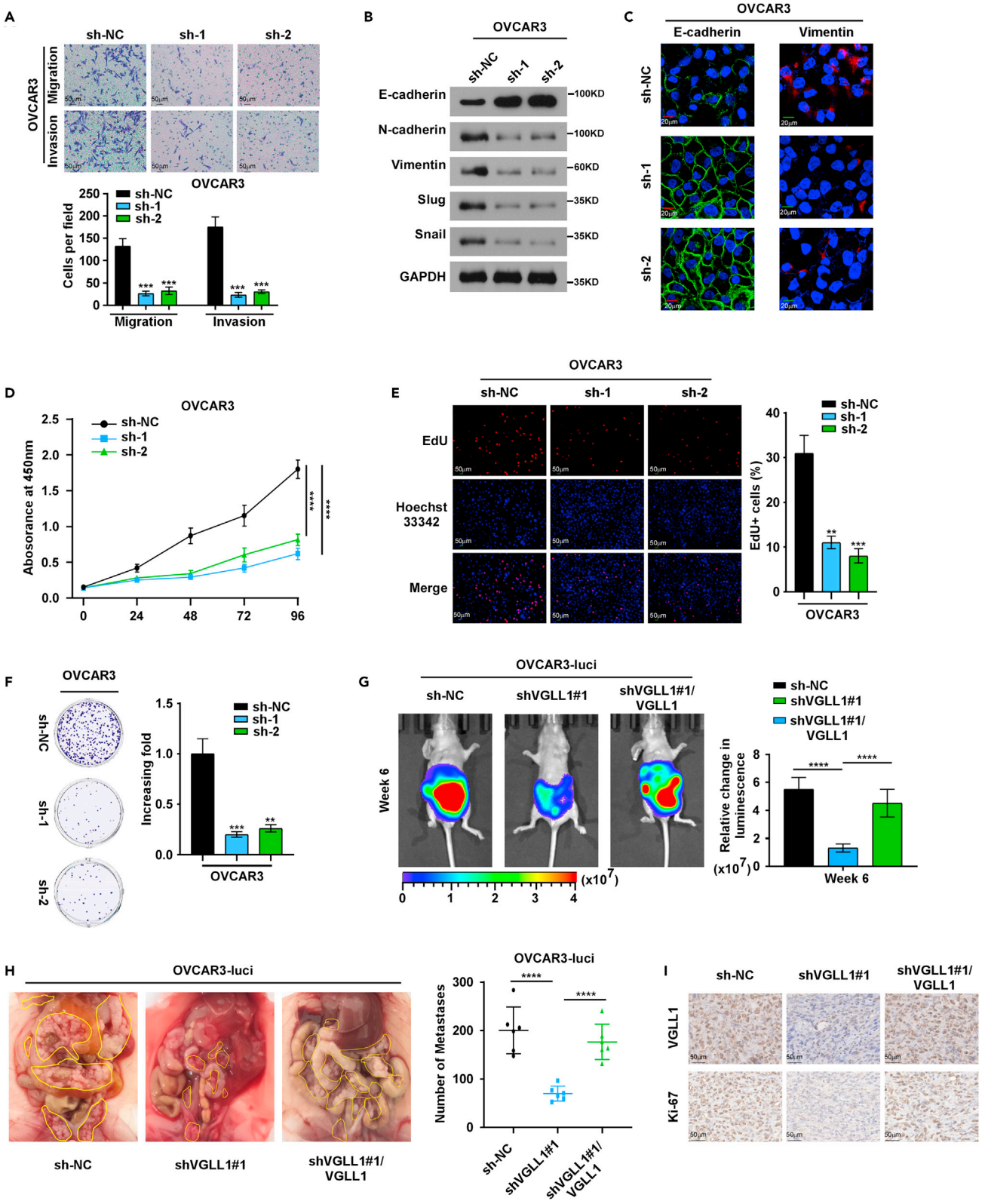
A
sh-NC
sh-1
sh-2
OVCAR3
Migration
Invasion
50μm
OVCAR3
Cells per field
250
200
150
100
50
0
sh-NC
sh-1
sh-2
***
Migration
Invasion
B
OVCAR3
sh-NC
sh-1
sh-2
E-cadherin
N-cadherin
Vimentin
Slug
Snail
GAPDH
100KD
100KD
60KD
35KD
35KD
35KD
C
OVCAR3
E-cadherin
Vimentin
sh-NC
sh-1
sh-2
20μm
D
OVCAR3
Absorance at 450nm
2.5
2.0
1.5
1.0
0.5
0.0
sh-NC
sh-1
sh-2
0
24
48
72
96
****
E
OVCAR3
sh-NC
sh-1
sh-2
EdU
Hoechst 33342
Merge
50μm
EdU+ cells (%)
40
30
20
10
0
**
***
OVCAR3
F
OVCAR3
sh-NC
sh-1
sh-2
Increasing fold
1.5
1.0
0.5
0.0
***
**
OVCAR3
G
OVCAR3-luci
sh-NC
shVGLL1#1
shVGLL1#1/ VGLL1
Week 6
(x10^7)
0
1
2
3
4
Relative change in luminescence
(x10^7)
8
6
4
2
0
****
****
Week 6
H
OVCAR3-luci
sh-NC
shVGLL1#1
shVGLL1#1/ VGLL1
Number of Metastases
300
200
100
0
****
****
I
sh-NC
shVGLL1#1
shVGLL1#1/ VGLL1
VGLL1
Ki-67
50μm

Figure 2. Inhibition of VGLL1 suppresses ovarian cancer cells metastasis

(A) Representative images of migration and invasion assays in OVCAR3 cells (Upper), Scale bar, 50 μm. Histogram analysis of migrated or invaded cell counts is shown (Bottom).

(B and C) EMT-related molecules detected by western blot and immunofluorescent staining in the indicated OVCAR3 cells, Scale bar, 20 μm.

(D) MTT assays assay was performed in the indicated cells.

(E) EdU assays in the indicated cells. Hoechst 33342 was stained used for nuclei in EdU assays. Error bars represent the mean ± SD of triplicate experiments. Scale bar, 50 μm.

(F) Colony formation assay was performed in the indicated cells.

(G) Representative images of intraperitoneal tumor-bearing mice in the indicated groups. (n = 6 mice/group).

(H) Intraperitoneal xenograft tumor formation in nude mice in indicated groups. Number of metastatic nodules is shown (mean ± SEM).

(I) IHC staining of VGLL1 and Ki-67 in the indicated group mice. Scale bar, 50 μm. Student's t tests were used for comparing two variables. The ANOVA test was used for multiple variable comparison. *$p < 0.05$, **$p < 0.01$, ***$p < 0.001$, ****$p < 0.0001$, ns indicates no significance. Each error bar represents the mean ± SD of three independent experiments.

in corresponding control cells. Western blotting showed that the silencing of VGLL1 significantly enhanced the level of E-cadherin but reduced the expression of the mesenchymal markers N-cadherin and vimentin, as well as EMT-activating transcription factors (EMT-TFs), such as SLUG and SNAIL; however, the upregulation of VGLL1 had the opposite effects (Figures 2B, S3A, and S3B). Moreover, the results of immunofluorescent staining were consistent with those of western blotting (Figures 2C, S3C, and S3D).

Compared with that in the control cells, the MTT proliferation rate was markedly decreased in *VGLL1*-knockdown A2780 and OVCAR3 cells (Figures 2D and S4A). *VGLL1* silencing-induced reductions in cell proliferation were further confirmed by colony formation and EdU assays. (Figures 2E, 2F, and S4B–S4D). In addition, we found that *VGLL1* overexpression had the opposite effect on OC cell proliferation (Figures S4E–S4J).

VGLL1 enhances ovarian cancer cell metastasis *in vivo*

To further investigate the effect of VGLL1 on OC tumor metastasis *in vivo*, the ovary of BALB/c nude mice was inoculated orthotopically with control or *VGLL1*-knockdown OVCAR3 cells. Intraperitoneal metastasis was monitored by the *in vivo* imaging system (IVIS). Mice orthotopically injected with VGLL1-knockdown OVCAR3 cells formed significantly fewer metastatic implants than the control mice (Figures 2G and 2H). Furthermore, omental tumors generated by VGLL1-knockdown OVCAR3 cells had lower levels of Ki-67 staining (Figure 2I). In contrast, re-overexpression of VGLL1 in OVCAR3-shVGLL1#1 cells restored the above effects of VGLL1 silencing on the intraperitoneal metastasis ability (Figure 2I). Moreover, as shown in Figure S5A, the mice bearing VGLL1-knockdown OVCAR3 cells showed a moderately decreased primary orthotopic tumor weight compared with the mice implanted with control OVCAR3 cells. The primary orthotopic tumor weight was moderately increased by re-expressing VGLL1 in the VGLL1-knockdown OVCAR3 cells. Consistent with the results of the metastasis site, silencing of VGLL1 in OVCAR3 cells significantly reduced, whereas the re-expressing of VGLL1 in OVCAR3 cells increased the expression of Ki-67, the mesenchymal markers N-cadherin and vimentin, SLUG, and SNAIL. However, silencing of VGLL1 in OVCAR3 cells increased the expression of E-cadherin, whereas re-expressing of VGLL1 in OVCAR3 cells decreased its expression (Figures S5B and S5C).

VGLL1 transcriptionally activates the high-mobility group AT-hook 1/β-catenin signaling pathway by interacting with TEAD4

To investigate the mechanism by which VGLL1 promotes OC malignant progression, we performed RNA-seq analyses in OVCAR3 cells (OVCAR3-shVGLL1#1 vs. OVCAR3 cells). After screening the transcriptional regulation prediction tool (chEA3[29] and hTFtarget[30]) and the RNA-seq data, we identified 2 mRNAs regulated by VGLL1 (Figure 3A). Next, we analyzed the clinical relevance between VGLL1 and HMGA1 and between VGLL1 and ZNF860 in patients with OC. We found that the expression of VGLL1 and HMGA1 was significantly positively correlated, while the correlation between VGLL1 and ZNF860 was not statistically significant (Figures 3B and 3C). Moreover, we also discovered that HMGA1 was highly expressed in metastatic OC tissues compared with primary OC tissues (Figure S6A). We analyzed the expression of these four TEADs, which contains a family of 4 transcription factors (TEAD1–4) that bind to a consensus DNA sequence 5′-CATTCC-3′ regulating cell growth, thereby leading to oncogenic transformation[31] in the OC dataset in the TCGA and GTEx databases. Interestingly, only *TEAD4* was overexpressed significantly in OC tissues compared with normal ovary tissues (Figures S6B–S6E). Immunoprecipitation (IP) and immunofluorescence assays validated the interaction between VGLL1 and TEAD4 (Figures 3D and 3E). Moreover, *in vitro* binding assays using purified proteins showed that VGLL1 interacted with TEAD4 directly (Figures S8A and S8B). The TEAD family plays an important role in tumor progression; therefore, we wondered whether the VGLL1/TEAD4 complex regulates the transcription of HMGA1. Moreover, HMGA1 was upregulated in *VGLL1*-overexpressing A2780 and OVCAR3 cells, as detected by western blot assays (Figure 3F). These results suggested that HMGA1 might be a potential downstream target of VGLL1. Additionally, *TEAD4* silencing reduced *VGLL1*-induced *HMGA1* promoter activity by luciferase activity assay (Figure 3G).

Moreover, JASPAR tool prediction based on published chromatin immunoprecipitation (ChIP-seq) data identified two potential VGLL1-TEAD4 binding sites in the HMGA1 promoter region. Luciferase reporter systems were then constructed comprising *HMGA1* promoters incorporating the wild-type binding site (wild), deletion of the binding site (del), and mutation of the binding site (mut). The degree of HMGA1 promoter activation was similar between the −1765 and −361 constructs, which suggested that the −1765 binding site is not essential for the binding of the VGLL1-TEAD4 complex to *HMGA1* (Figure 3H). Moreover, endogenous VGLL1 could bind the putative binding site

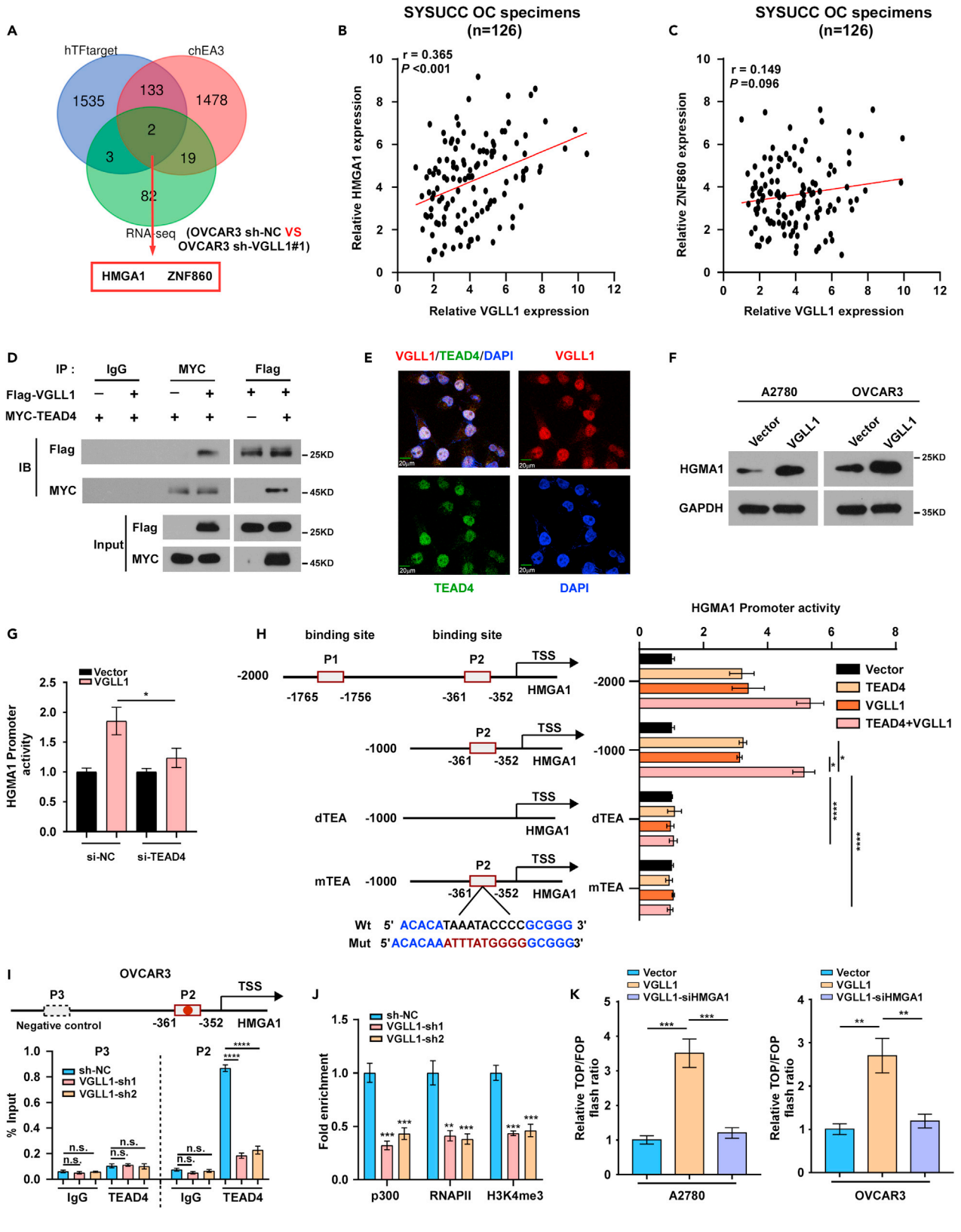
A
hTFtarget
chEA3
1535
133
1478
2
3
19
82
RNA-seq (OVCAR3 sh-NC VS OVCAR3 sh-VGLL1#1)
HMGA1 ZNF860
B
SYSUCC OC specimens (n=126)
r = 0.365
P <0.001
Relative HMGA1 expression
Relative VGLL1 expression
C
SYSUCC OC specimens (n=126)
r = 0.149
P =0.096
Relative ZNF860 expression
Relative VGLL1 expression
D
IP : IgG MYC Flag
Flag-VGLL1
MYC-TEAD4
IB
Flag
MYC
Input
25KD
45KD
E
VGLL1/TEAD4/DAPI
VGLL1
TEAD4
DAPI
F
A2780
OVCAR3
Vector
VGLL1
HGMA1
GAPDH
25KD
35KD
G
Vector
VGLL1
HGMA1 Promoter activity
si-NC
si-TEAD4
H
binding site
binding site
P1
P2
TSS
HMGA1
-2000
-1765
-1756
-361
-352
-1000
dTEA
mTEA
Wt 5' ACACATAAATACCCCGCGGG 3'
Mut 5'ACACAAATTTATGGGGCGCGG3'
HGMA1 Promoter activity
Vector
TEAD4
VGLL1
TEAD4+VGLL1
I
OVCAR3
P3
P2
TSS
Negative control
HMGA1
% Input
sh-NC
VGLL1-sh1
VGLL1-sh2
n.s.
IgG
TEAD4
J
Fold enrichment
p300
RNAPII
H3K4me3
K
Vector
VGLL1
VGLL1-siHMGA1
Relative TOP/FOP flash ratio
A2780
OVCAR3

Figure 3. VGLL1 transcriptionally activates HMGA1 via interacting TEAD4

(A) Flowing chart illustrates the criteria for identifying of HMGA1 as the target of VGLL1.

(B) The clinical correlation between VGLL1 expression and HMGA1 expression (Pearson correlation test).

(C) The clinical correlation between VGLL1 expression and ZNF860 expression (Pearson correlation test).

(D) Interaction between VGLL1 and TEAD4. Lysates of A2780 cells that were transfected with pcDNA3.1-Flag-VGLL1 and pcDNA3.1-myc-TEAD4 were immunoprecipitated using anti-IgG, anti-Flag, and anti-Myc antibodies. Protein expression was analyzed by immunoblotting.

(E) IF assay showing that VGLL1 is colocalized with TEAD4 in the nucleus. Scale bar, 20 μm.

(F) HMGA1 expression levels in the indicated A2780 and OVCAR3 cells examined by western blot assay.

(G) Effect of TEAD4 on VGLL1-regulated HMGA1 transcriptional activity.

(H) HMGA1 promoter activities of the reporter systems containing modified binding sites were measured in OVCAR3 cells.

(I) Schematic illustration of the human *HMGA1* gene promoter (upper panel) and ChIP analysis of enrichment of TEAD4 on the HMGA1 promoter (lower panel). IgG was used as a negative control. The qRT–PCR amplification regions are shown in red squares.

(J) ChIP assays were performed in the indicated cells using anti-p300 acetyltransferase, anti-RNA POL II (RNAP II), and anti-H3K4me3 antibodies.

(K) TOP/FOP luciferase activity in the indicated cells. Student's t tests were used for comparing two variables. *$p < 0.05$, **$p < 0.01$, ***$p < 0.001$, ****$p < 0.0001$, ns indicates no significance. Each error bar represents the mean ± SD of three independent experiments.

(−361 to −352 constructs) on the HMGA1 promoter region, while knockdown of VGLL1 strongly decreased the enrichment of p300, RNA polymerase II, and H3K4me3 on the HMGA1 promoter, as examined by ChIP assays (Figures 3I and 3J). These results suggested that VGLL1 serves as a cofactor of TEAD4, which binds to the −361 site in the HMGA1 promoter.

Previous studies have shown that the HMGA1-mediated activation of Wnt/β-catenin signaling enhances tumor progression.[32] We found that VGLL1 elevation markedly increased β-catenin/TCF transcriptional activity. In contrast, the knockdown of HMGA1 significantly repressed β-catenin/TCF transcriptional activity (Figure 3K). Next, we measured the expression of *c-MYC, MMP7,* and *MMP9*, three typical β-catenin downstream genes, using qRT-PCR and western blot analysis. *c-MYC, MMP7,* and *MMP9* mRNA expression increased significantly when *VGLL1* was overexpressed, and silencing HMGA1 expression reversed this effect (Figures S7A and S7B). These results were also verified in the indicated OVCAR3 tumors (Figure S7C).

High-mobility group AT-hook 1 is essential for VGLL1-mediated metastasis in ovarian cancer

We further investigated the role of HMGA1 in VGLL1-mediated metastasis in OC. Additionally, we also conducted several *in vitro* assays, including invasion, migration assays, and EMT assays, and the results showed that knockdown of HMGA1 expression significantly inhibited the effects of *VGLL1* overexpression (Figures 4A–4D, and S9A). Moreover, colony formation assays and EdU assays also demonstrated that silencing HMGA1 expression obviously repressed the proliferation effects mediated by high expression of VGLL1 (Figures 4E and 4F). Moreover, the numbers of intraperitoneal metastatic nodules were decreased significantly in the OVCAR3-VGLL1 group upon silencing HMGA1 expression (Figures 4G and 4H). We also discovered that the upregulation of VGLL1 increased the nuclear translocation of β-catenin in A2780 cells, and nuclear translocation of β-catenin was decreased upon the silencing of HMGA1 expression, as detected by the immunoblotting of nuclear and cytoplasmic cellular fractions and immunofluorescent staining (Figures 4I and S10A).

To further explore whether β-catenin activation was responsible for the VGLL1-mediated effects, we determined the impact of blocking the Wnt/β-catenin pathway on the metastasis of OC cells using the tankyrase inhibitor XAV-939 (S1180, Selleck). As shown in Figures 4J−4L, VGLL1-induced invasion, migration, and proliferation in OC cells were repressed by XAV939 treatment.

METTL3-mediated N^6-methyladenosine modification contributes to the upregulation of VGLL1 in ovarian cancer

Recent advances have suggested that cancer progression is frequently induced by both genetic and epigenetic modifications.[33] Therefore, we explored the mechanism that induces *VGLL1* upregulation in OC. First, using the "Ovarian Epithelial Carcinoma (TCGA, Provisional)" dataset from the cBioPortal database (http://www.cbioportal.org), we investigated the correlation between mRNA expression and the genomic copy number of *VGLL1*. However, the results showed that the overexpression of *VGLL1* in OC was not affected significantly by genetic amplification (Figure S11A). Emerging studies have indicated that epigenetic modifications are frequently involved in the dysregulation of mRNA. Thus, we wondered whether epigenetic modification induced *VGLL1* upregulation in OC. Treatment of OC cells with a broad-spectrum HDAC inhibitor (SAHA and NaB) or DNA methyltransferase inhibitor (5-zaz-dC) were used to detect the DNA methylation or histone acetylation level of *VGLL1* in A2780 and OVCAR3 cells (Figures 5A, 5B, and S11B), and the results showed that DNA methylation and histone acetylation did not contribute to the upregulation of *VGLL1* in OC cells.

Recent advances have indicated that m^6A is the most abundant modification in mRNA, mediated by "writers," inhibited by "erasers," and functionally executed by readers.[34] Therefore, we explored whether m^6A modification is involved in *VGLL1* upregulation. An online m^6A site predictor, SRAMP,[35] showed that several m^6A sites were located in *VGLL1* (Figure 5C). To investigate which m^6A site is responsible for m^6A-mediated *VGLL1*stabilization, seven VGLL1 mutants were designed, and luciferase reporter assay was performed (Figure S12A). Our results indicated that site 2('AAGGGGACA') and site 4('CCAUGGACA') were involved in regulating VGLL1 stability (Figure S12B). Moreover, the m^6A level of *VGLL1* was upregulated in A2780 and OVCAR3 cells compared with that in the normal ovarian epithelial cell line Hosepic (Figure 5D). Further assessment of the expression of m^6A WERs in OC tissues obtained from SYSUCC (Sun Yat-sen University Cancer Center) showed significant increases in the expression levels of *METTL3, YTHDC1,* and *IGF2BP2* in OC tissues and IGF2BP1 was downregulated in OC samples, whereas the expression levels of other WREs showed no differences (Figures 5E–5I and S11C−S11H). Moreover, the protein levels of METTL3

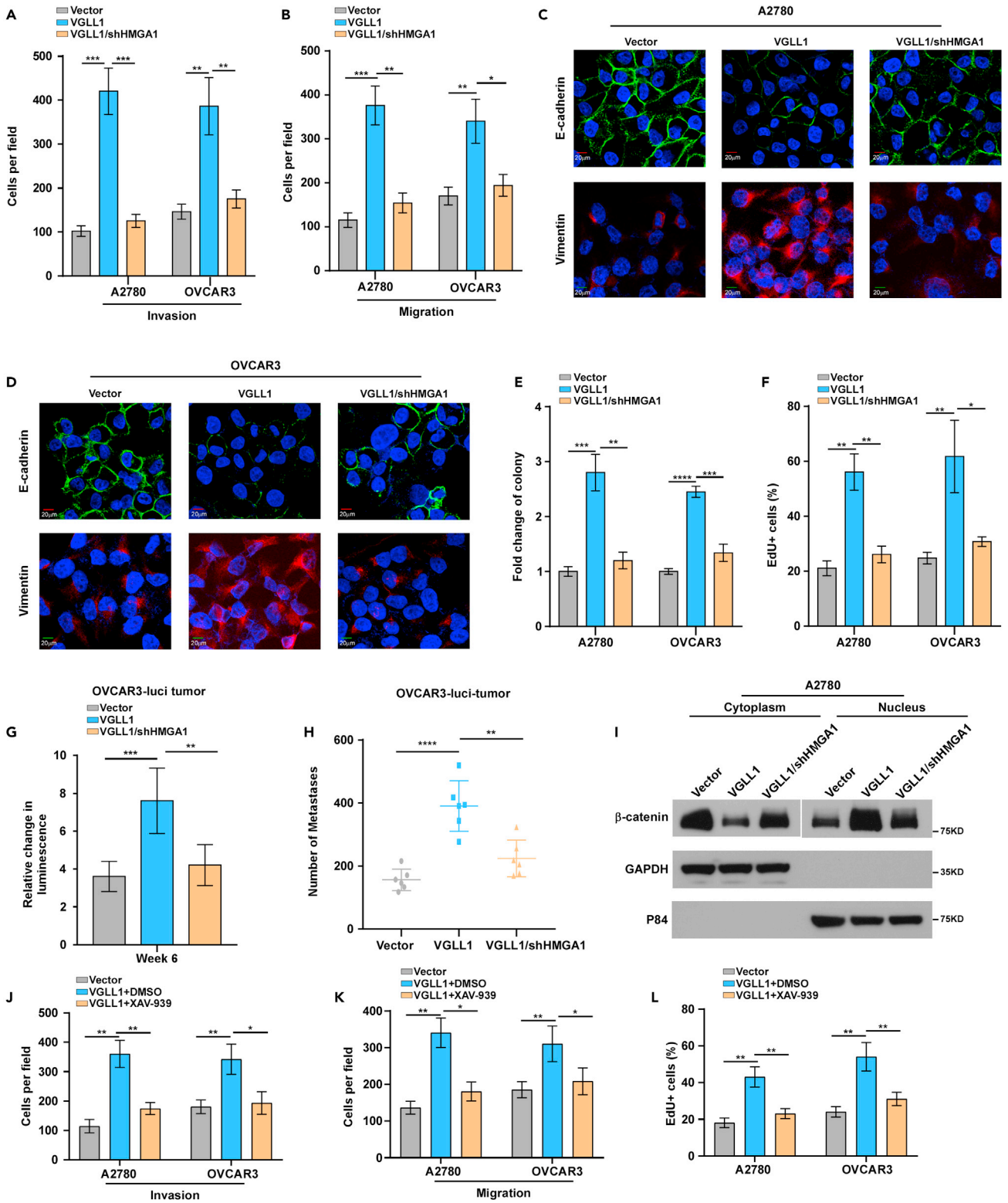

Figure 4. HMGA1 is essential for VGLL1-mediated proliferation and metastasis in ovarian cancer

(A) Quantification of cell invasiveness determined by transwell assays in the indicated cells.

(B) Quantification of migrated cells determined by transwell assay using indicated cells.

Figure 4. *Continued*

(C and D) Immunofluorescence images of EMT-associated factors, E-cadherin and vimentin using the indicated cells. E-cadherin was stained green, Vimentin was stained red, and nuclei was stained with DAPI were blue. Scale bar, 20 μm.

(E) Quantification of colony formation ability in the indicated cells.

(F) Quantification of EdU positive cells in the indicated cells.

(G and H) Quantification of the relative change in luminescence (G) and number of metastases (H) of mice from the indicated groups.

(I) Western blotting analysis of β-catenin expression in the cytoplasm and nucleus of the indicated cells. GADPH and p84 were used as loading controls for the cytoplasmic and nuclear fractions, respectively.

(J) Quantification of cell invasiveness determined by transwell assays in the indicated cells.

(K) Quantification of migrated cells determined by transwell assay using indicated cells.

(L) Quantification of EdU positive cells in the indicated cells. Student's t tests were used for comparing two variables. *$p < 0.05$, **$p < 0.01$, ***$p < 0.001$, ****$p < 0.0001$, ns indicates no significance. Each error bar represents the mean ± SD of three independent experiments.

and IGF2BP2 were significantly increased in the OC tissues compared to those in normal ovary tissues (Figures S13A and S13B). Previous studies indicated that the IGF2BP family recognized m^{6}A-modified mRNAs and sustained their stability to promote cancer progression.[34] To identify the specific m^{6}A reader of *VGLL1* and determine the m^{6}A-modification mechanism of *VGLL1* upregulation, a streptavidin RNA pull-down assay to screen for *VGLL1*-related m^{6}A readers was conducted. We found that IGF2BP2, but not the other members of the IGF2BP family (IGF2BP1) or the YTH family (e.g., YTHDF1/2/3, YTHDC1), directly bound to the full-length transcripts in A2780 and OVCAR3 cells (Figures 5J, 5K, and S11K). Moreover, RIP-PCR experiments also revealed that *VGLL1* mRNA levels were significantly increased in RNA precipitated by METTL3 and IGF2BP2 antibodies compared with that precipitated by IgG in A2780 and OVCAR3 cells, whereas its cannot be precipitated by IGF2BP1 antibody (Figures 5L, 5M, and S11J). Furthermore, we also evaluated RNA expression after METTL3 or IGF2BP2 knockdown in OC cells. The mRNA level of *VGLL1* was markedly decreased after METTL3 or IGF2BP2 silencing in A2780 and OVCAR3 cells treated with Actinomycin D (5 μg/mL) (Figures 5N–5Q).

Inducible silencing of *VGLL1* abrogates ovarian cancer metastasis

Finally, we evaluated whether targeting *VGLL1* might abrogate metastasis in OC. A doxycycline (Dox)-induced knockdown system was used to conditionally knock down *VGLL1* in OC cells (Figure 6A). The migration ability, surviving colony ability, and proliferation capacity were robustly impaired in *VGLL1*-silenced OC cells, indicating that *VGLL1* was required for these processes (Figures S14A–S14H).

The therapeutic potential of *VGLL1* was further assessed *in vivo* using xenograft models. Briefly, mice were randomly divided into two groups (n = 6/group) and inoculated orthotopically with OVCAR3-shVGLL1^{DOX} cells. After 10 days of inoculation, one group of mice was fed drinking water containing Dox to induce *VGLL1* downregulation in tumors (Figure 6B). The growth and metastasis of tumors were recorded. Notably, Dox-induced silencing of *VGLL1* significantly reduced the growth and metastasis rate of tumors, suggesting that the upregulation of *VGLL1* was essential for OC tumor growth and metastasis. (Figures 6C–6E).

Likewise, silencing IGF2BP2 potently impaired VGLL1 expression in OVCAR3 cells. Consistent with the above results, the knockdown of IGF2BP2 significantly repressed the migration ability, colony formation ability, and proliferation capacity (Figures S15A–S15H). Moreover, the knockdown of IGF2BP2 or METTL3 obviously repressed the growth and metastasis rate of tumors. These results indicated that IGF2BP2 or METTL3 were required for VGLL1 upregulation (Figures 6F–6H and S16A–S16D).

Clinical relevance of the METTL3-mediated N^6-methyladenosine/VGLL1/high-mobility group AT-hook 1 axis in ovarian cancer

Based on the mechanism we investigated above, we further proceeded to explore the clinical relevance among IGF2BP2, VGLL1, β-catenin, and HMGA1 in OC specimens. IHC assays showed that IGF2BP2, VGLL1, β-catenin, and HMGA1 expression was potently upregulated in OC specimens with metastasis compared with those without metastasis (Figure 6I). Notably, VGLL1 expression was positively correlated with IGF2BP2, HMGA1, and nuclear β-catenin in OC tissues (Figures 6J–6L).

In summary, our findings showed that methylated *VGLL1* was subsequently recognized by the m^{6}A "reader IGF2BP2 to maintain its mRNA stability and contribute to its upregulation. Increasing the *VGLL1* expression level promoted OC cell metastasis by activating the VGLL1/HGMA1/β-catenin axis (Figure 6M).

DISCUSSION

The overall five-year patient survival rate for OC is only 40%, mainly because of its advanced stage at diagnosis and the propensity for peritoneal cavity metastasis, even when the primary tumors are small.[1] Peritoneal metastasis occurs in almost all patients with OC, especially at the advanced stage, finally causing death.[3] Moreover, treatment for peritoneal cavity metastasis has limited effects in the clinic.[36] Therefore, the exploration of the mechanism of peritoneal metastasis is essential to improving the clinical outcome of patients with OC. Although well-established studies have indicated that m^{6}A methylation modification has a broad impact on cancer progression and precision therapy,[22,26] the relationship between m^{6}A methylation modification and peritoneal metastasis of OC has not been well studied thus far. This study identified that VGLL1 was increased in peritoneally metastatic OC and predicted a poor prognosis. Furthermore, VGLL1 knockdown inhibited the metastasis of OC cells. Mechanistically, m^{6}A modification of VGLL1 stabilized its mRNA recognized by

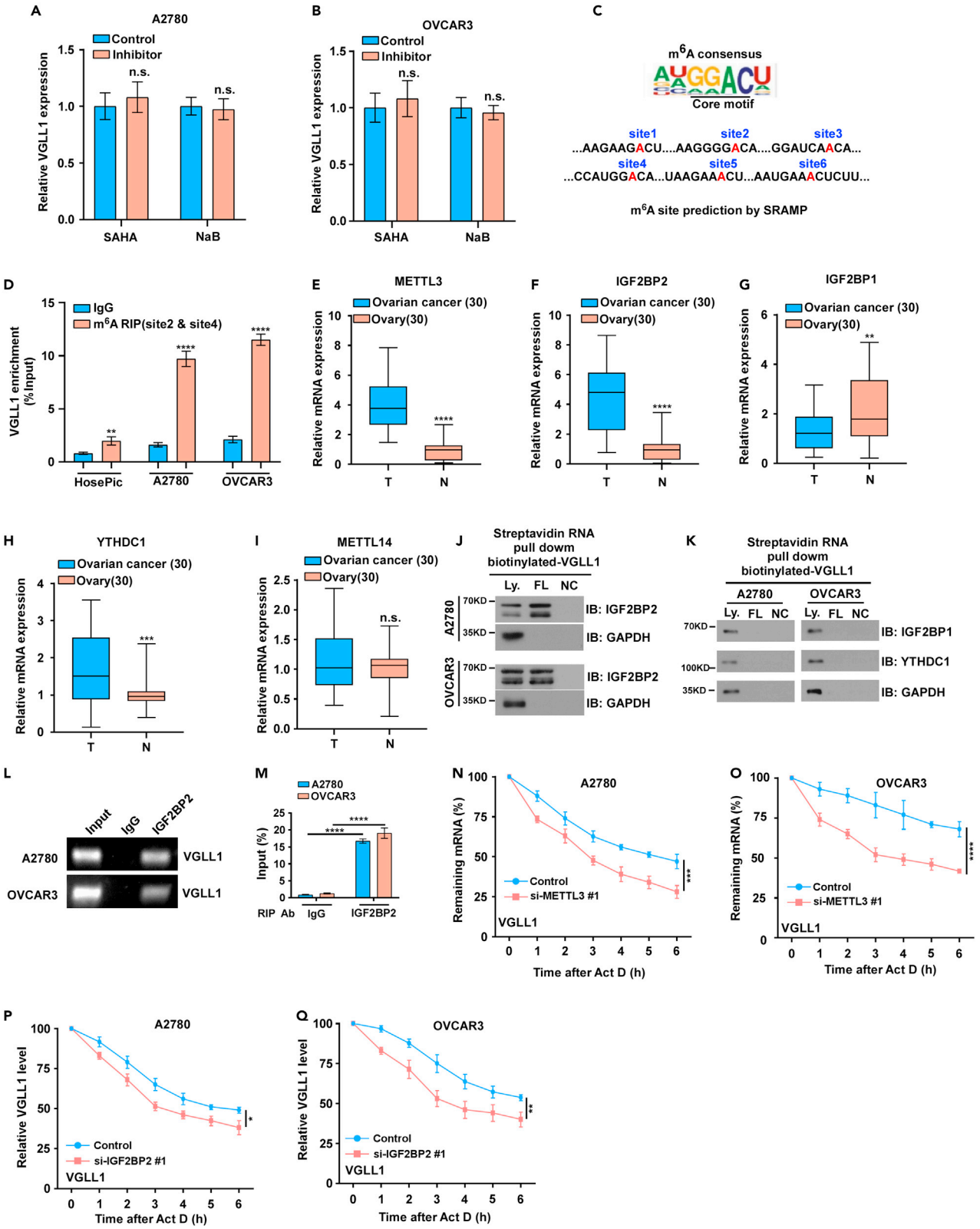
A
A2780
Control
Inhibitor
n.s.
n.s.
Relative VGLL1 expression
SAHA
NaB
B
OVCAR3
C
m6A consensus
Core motif
site1
site2
site3
...AAGAAGACU....AAGGGGACA....GGAUCAACA...
site4
site5
site6
...CCAUGGACA...UAAGAAACU...AAUGAACUCUU...
m6A site prediction by SRAMP
D
IgG
m6A RIP(site2 & site4)
VGLL1 enrichment (%Input)
HosePic
A2780
OVCAR3
E
METTL3
Ovarian cancer (30)
Ovary(30)
Relative mRNA expression
T
N
F
IGF2BP2
G
IGF2BP1
H
YTHDC1
I
METTL14
J
Streptavidin RNA pull dowm biotinylated-VGLL1
Ly.
FL
NC
70KD
35KD
IB: IGF2BP2
IB: GAPDH
K
A2780
OVCAR3
100KD
IB: IGF2BP1
IB: YTHDC1
L
Input
IgG
IGF2BP2
VGLL1
M
Input (%)
RIP Ab
N
Remaining mRNA (%)
Control
si-METTL3 #1
Time after Act D (h)
O
P
Relative VGLL1 level
si-IGF2BP2 #1
Q

Figure 5. m^{6}A modification contributes to the upregulation of VGLL1 in OC

(A and B) qRT-PCR analysis of *VGLL1* expression in A2780 and OVCAR3 cells with or without the treatment of SAHA or NaB. Transcript levels were normalized to GAPDH expression. Error bars represent the mean ± SD of triplicate experiments.

(C) The putative wild-type m^{6}A sites and designed mutant m^{6}A sites in *VGLL1*.

(D) m^{6}A RIP-qPCR analysis of *VGLL1* in HosePic, A2780 and OVCAR3 cells. Error bars represent the mean ± SD of triplicate experiments.

(E–I) qRT-PCR analysis of m^{6}A WER expression in 30 OC tumor tissues and 30 normal ovary tissues.

(J and K) Immunoblotting of IGF2BP2, IGF2BP1, and YTHDC1 after RNA pull down assay with cell lysate (Ly.), full-length biotinylated- *VGLL1* (FL), and beads only (NC) in A2780 and OVCAR3 cells.

(L and M) Agarose electrophoresis and qRT-PCR analysis of RIP assays in A2780 and OVCAR3 cells showing the direct binding between the IGF2BP2 protein and *VGLL1* mRNA.

(N–Q) qRT-PCR analysis of *VGLL1* at the indicated times after actinomycin D (5 μg/mL) treatment in A2780 and OVCAR3 cells after METTL3 inhibition (N, O), and in A2780 and OVCAR3 cells after IGF2BP2 inhibition (P, Q). Student's t tests were used for comparing two variables. The ANOVA test was used for multiple variables comparison. **p < 0.01, ***p < 0.001, ****p < 0.0001, ns indicates no significance. Each error bar represents the mean ± SD of three independent experiments.

IGF2BP2, a proven m^{6}A reader, further activating HMGA1/Wnt/β-catenin signaling. These findings revealed an important role of VGLL1 in promoting metastasis of OC, and suggested that VGLL1 as a promising prognostic biomarker and potential target in OC, especially for metastatic patients with OC.

The metastatic tropism of OC cells, by which they spread directly into adjacent organs, especially in the fallopian tubes, uterus, and gastrointestinal system, is unique.[2] Hanahan et al. reported that epithelial tumor cells must acquire invasive properties to disseminate and develop new tumor nodules in the peritoneal cavity or at distant sites.[37] Tumor cells undergo EMT during the metastasis process, losing cell–cell contacts and subsequently reducing the expression of E-cadherin and increasing the expression levels of several invasion and migration markers.[38] These studies emphasize the important role of EMT properties in tumor metastasis. However, the mechanism by which EMT progression is regulated in OC remains elusive. In this study, our data show that VGLL1 enhances EMT properties in OC cells to further promote metastasis. Conversely, the inhibition of VGLL1 is regulated by m^{6}A modification to reduce EMT progression and metastasis capacity in OC cells.

Recently, several studies reported that high-mobility group AT-hook 1 (HMGA1) contributes to tumor progression and metastatic processes in cancers via EMT.[39] However, the function and detailed understanding of the molecular mechanisms of HMGA1 in OC cell metastasis, especially transcoelomic metastasis, are still unclear. Belton et al. reported that HMGA1 contributes to cell proliferation and polyp formation in the intestines and ultimately induces metastatic development in colon cancer cells.[40] Previous studies have shown that HMAG1 activates the Wnt/β-signaling pathway at multiple levels. First, HMGA1 upregulates the expression of Wnt agonist receptor genes and increases Wnt/TCF4/β-catenin downstream effector genes. Second, TCF4 and HMGA1 form a "feedforward loop," in which TCF4 binds to the HMGA1 promoter, and TCF4/β-catenin upregulates HMGA1, which induces Wnt/β-catenin signaling activation. Third, HMGA1 leads to the inhibition of GSK3-mediated β-catenin phosphorylation and stabilization, which then induce β-catenin nuclear translocation.[41] Activation of Wnt/β-catenin signaling contributes to enhanced invasion and migration capacity in gynecologic malignancies, including OC.[42] Moreover, Wnt/β-catenin signaling is implicated in cancer cell colonization, survival, and proliferation, which are critical steps of cancer metastasis[43] In this study, we revealed that OC cells with high HMGA1/Wnt/β-catenin activated levels, regulating by VGLL1 overexpression, tended to metastasize and form peritoneal metastatic tumors. Therefore, HMGA1/Wnt/β-catenin signaling is critical in VGLL1-induced metastasis of OC, which suggests that a Wnt/β-catenin inhibitor (XAV-939) may be a potentially effective therapeutic strategy for patients with OC with increased VGLL1 expression.

VGLL1 overexpression has been shown to correlate with a poorer prognosis and shorter survival in multiple types of cancer.[19,20] VGLL1 functions as a co-transcriptional activator and a driver of metastasis and proliferation during human cancer development via interaction with the transcription factor TEAD4.[44,45] VGLL1 interacts with TEAD4 in a similar manner to YAP/TAZ binding to TEAD proteins, which results in the upregulation of IGFBP5, a proliferation-promoting protein.[45] These observations regarding VGLL1 prompted us to explore its precise role in OC metastasis. In this study, our data suggested that VGLL1 directly interacts with TEAD4 to transcriptionally activate HMGA1/Wnt/β-catenin signaling, ultimately promoting OC cell metastasis. Therefore, we speculated that VGLL1 might serve as a valuable biomarker and therapeutic target in metastatic OC.

M^{6}A is a widely prevalent the posttranscriptional modification of RNA that controls RNA metabolism at multiple levels.[46] Zhou et al. found that FTO reduced the β-catenin m^{6}A modification level, increased its expression, and increased ERCC excision repair 1 (ERCC1) expression. A study by Liu T et al. showed that YTHDF1 promotes OC metastasis and progression by increasing eIF3C translation in a m^{6}A-dependent manner.[23] Similarly, our data indicated that the m^{6}A modification caused the upregulation of *VGLL1*. Further exploration showed that METTL3 functions as a m^{6}A writer for *VGLL1* and is recognized by the classic m^{6}A reader IGF2BP2, which has been reported to promote the stability of mRNA. Hou P et al. found that IGF2BP2 recognized m^{6}A-modified *HTR3A* to stabilize its mRNA, which promoted metastasis and proliferation of esophageal squamous cell carcinoma.[47] Consistent with previous studies, we found that IGF2BP2 or METTL3 knockdown remarkably reduced the half-life of *VGLL1* in an m^{6}A modification manner. In this study, we found that VGLL1 was increased in OCOC with peritoneal metastasis and was correlated with a poor prognosis in patients with OC. Furthermore, functional assays indicated that VGLL1 knockdown inhibited metastasis and tumor growth in OC cells. Mechanistically, upregulation of VGLL1 was mediated by m^{6}A modification and then induced OC cell metastasis by forming the VGLL1/HMGA1/β-catenin signaling axis.

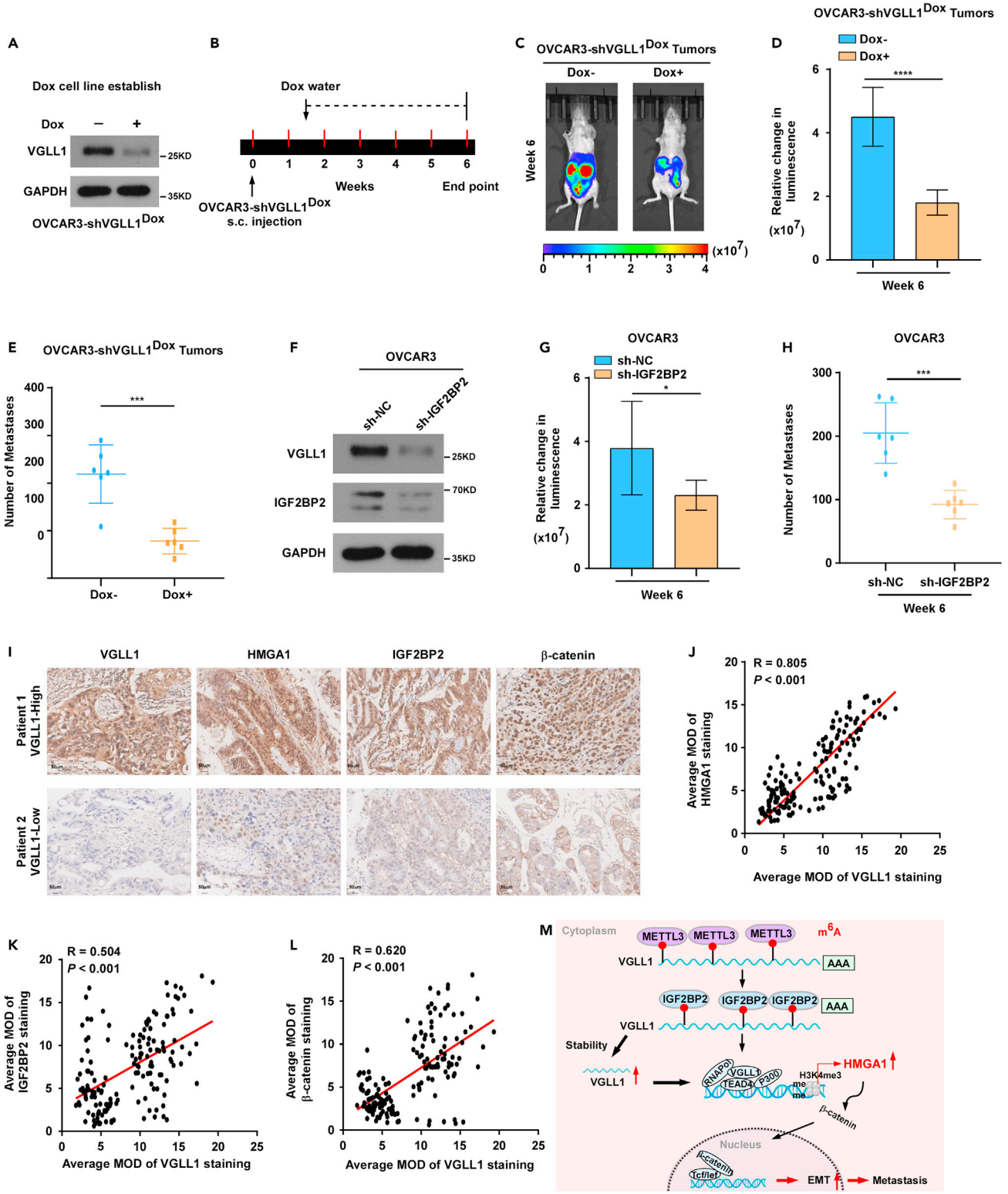

Figure 6. Inducible silencing of VGLL1 abrogates metastasis of OC and Clinical relevance of m^{6}A/VGLL1/HMGA1 axis in OC

(A) Western blotting analysis of VGLL1 to verify that VGLL1 can be conditionally silenced via doxycycline treatment (Dox, 100 ng/mL) in OVCAR3-shVGLL1^{Dox} cells.

(B) Scheme for the mice model.

(C and D) Tumors from indicated groups were shown (n = 6 mice/group).

Figure 6. *Continued*

(E) Quantification of ovarian metastasis nodules in the peritoneal cavity.

(F) Western blotting analysis of VGLL1 and IGF2BP2 in the indicated cells.

(G) Representative images of intraperitoneal tumor-bearing mice in the indicated groups. (n = 6 mice/group).

(H) Quantification of ovarian metastasis nodules in the peritoneal cavity.

(I) Representative images showing high or low expression of VGLL1, METTL3, IGF2BP2, and β-catenin in OC tissues. Scale bar, 50 μm.

(J–L) Correlation between VGLL1, METTL3, IGF2BP2, and β-catenin in 157 OC tumor tissue specimens (Pearson correlation test).

(M) Working model of the mechanism proposed in this study. Student's t tests were used for comparing two variables. *$p < 0.05$, ***$p < 0.001$, ****$p < 0.0001$, ns indicates no significance. Each error bar represents the mean ± SD of three independent experiments.

Conclusions

In summary, our findings reveal that m^{6}A-modified *VGLL1* is recognized by IGF2BP2, which stabilizes *VGLL1* mRNA, thereby promoting tumor growth and transcoelomic metastasis of OC cells. The study uncovers a detailed mechanism for transcoelomic metastasis in OC cells. Our work also suggests that VGLL1 may serve as a promising prognostic marker and a valuable therapeutic strategy against the transcoelomic metastasis of OC.

Limitations of the study

In this study, we found that m^{6}A-modified *VGLL1* is recognized by IGF2BP2, which stabilizes *VGLL1* mRNA, thereby promoting tumor growth and transcoelomic metastasis of OC cells. The detailed mechanism still remains to be further investigated. Also, the current study falls short of evaluating the potential target for individualized therapy of the VGLL1/HMGA1/β-catenin signaling axis.

STAR★METHODS

Detailed methods are provided in the online version of this paper and include the following:

- KEY RESOURCES TABLE
- RESOURCE AVAILABILITY
  - Lead contact
  - Materials availability
  - Data and code availability
- EXPERIMENTAL MODEL AND STUDY PARTICIPANT DETAILS
  - Cell lines and cell culture
  - Xenograft tumor models
  - Patient specimens
- METHOD DETAILS
  - RNA isolation, reverse transcription and qRT–PCR
  - RNA sequencing
  - Wound healing assay
  - mRNA stability assay
  - Protein immunoprecipitation (IP) assays
  - RNA immunoprecipitation (RIP) assays
  - Immunohistochemistry (IHC)
  - Mean optical density (MOD) analysis
  - Western blot analysis
  - Transwell matrix invasion assay
  - Immunofluorescence
  - Cell proliferation assays
  - TOP/FOP flash activity assays
  - Methylated RNA immunoprecipitation (MeRIP)
  - Luciferase activity assay
  - DNA constructs and establishment of stable cell lines
  - Chromatin immunoprecipitation (ChIP) assay
- QUANTIFICATION AND STATISTICAL ANALYSIS

SUPPLEMENTAL INFORMATION

Supplemental information can be found online at https://doi.org/10.1016/j.isci.2024.109245.

ACKNOWLEDGMENTS

We thank the specialists from Sun Yat-sen University Cancer Center for their technical supports of this work. This work was supported by the National Key R&D Program of China (grant number 2018YFC1313400); Science and Technology Planning Project of Guangdong Province, China (grant number 2017B020227003).

AUTHOR CONTRIBUTIONS

H.L., L.M. C., and Q.Z. P. carried out most of the experimental work, they collected and analyzed the data. X.Y.J., J.J. Z., and D.S.W. collected tissues, patient information, and conducted IHC and survival analysis. Q.Z. P., T. X., Y.T., Q.J.W., and J.H. conducted the western blot analysis, plasmid constructions, and cell culture. Z.Q. L. and J.C.X. raised the concept, design the experiments, wrote the article, and supervised the project. All authors reviewed the article.

DECLARATION OF INTERESTS

The authors declare no conflict of interest.

Received: July 17, 2023
Revised: November 30, 2023
Accepted: February 13, 2024
Published: February 16, 2024

REFERENCES

1. Coleman, R.L. (2016). Ovarian cancer in 2015: Insights into strategies for optimizing ovarian cancer care. Nat. Rev. Clin. Oncol. *13*, 71–72.
2. Tan, D.S.P., Agarwal, R., and Kaye, S.B. (2006). Mechanisms of transcoelomic metastasis in ovarian cancer. Lancet Oncol. *7*, 925–934.
3. Lengyel, E. (2010). Ovarian cancer development and metastasis. Am. J. Pathol. *177*, 1053–1064.
4. Reid, B.M., Permuth, J.B., and Sellers, T.A. (2017). Epidemiology of ovarian cancer: a review. Cancer Biol. Med. *14*, 9–32.
5. Gupta, G.P., and Massagué, J. (2006). Cancer metastasis: building a framework. Cell *127*, 679–695.
6. Shield, K., Ackland, M.L., Ahmed, N., and Rice, G.E. (2009). Multicellular spheroids in ovarian cancer metastases: Biology and pathology. Gynecol. Oncol. *113*, 143–148.
7. Eskander, R.N., and Tewari, K.S. (2012). Emerging treatment options for management of malignant ascites in patients with ovarian cancer. Int. J. Womens Health *4*, 395–404.
8. Sampson, J.A. (1931). Implantation Peritoneal Carcinomatosis of Ovarian Origin. Am. J. Pathol. *7*, 423–444.
9. Brabletz, T., Kalluri, R., Nieto, M.A., and Weinberg, R.A. (2018). EMT in cancer. Nat. Rev. Cancer *18*, 128–134.
10. Pastushenko, I., and Blanpain, C. (2019). EMT Transition States during Tumor Progression and Metastasis. Trends Cell Biol. *29*, 212–226.
11. Tam, W.L., and Weinberg, R.A. (2013). The epigenetics of epithelial-mesenchymal plasticity in cancer. Nat. Med. *19*, 1438–1449.
12. Yang, J., and Weinberg, R.A. (2008). Epithelial-mesenchymal transition: at the crossroads of development and tumor metastasis. Dev. Cell *14*, 818–829.
13. Hu, L., Ding, M., and He, W. (2021). Emerging Therapeutic Strategies for Attenuating Tubular EMT and Kidney Fibrosis by Targeting Wnt/beta-Catenin Signaling. Front. Pharmacol. *12*, 830340.
14. Nwabo Kamdje, A.H., Takam Kamga, P., Tagne Simo, R., Vecchio, L., Seke Etet, P.F., Muller, J.M., Bassi, G., Lukong, E., Kumar Goel, R., Mbo Amvene, J., and Krampera, M. (2017). Developmental pathways associated with cancer metastasis: Notch, Wnt, and Hedgehog. Cancer Biol. Med. *14*, 109–120.
15. Dongre, A., and Weinberg, R.A. (2019). New insights into the mechanisms of epithelial-mesenchymal transition and implications for cancer. Nat. Rev. Mol. Cell Biol. *20*, 69–84.
16. Vaudin, P., Delanoue, R., Davidson, I., Silber, J., and Zider, A. (1999). TONDU (TDU), a novel human protein related to the product of vestigial (vg) gene of Drosophila melanogaster interacts with vertebrate TEF factors and substitutes for Vg function in wing formation. Development *126*, 4807–4816.
17. Simon, E., Faucheux, C., Zider, A., Thézé, N., and Thiébaud, P. (2016). From vestigial to vestigial-like: the Drosophila gene that has taken wing. Dev. Genes Evol. *226*, 297–315.
18. Yamaguchi, N. (2020). Multiple Roles of Vestigial-Like Family Members in Tumor Development. Front. Oncol. *10*, 1266.
19. Komatsu, M., Kawamoto, T., Kanzawa, M., Kawakami, Y., Hara, H., Akisue, T., Kuroda, R., Nakamura, H., Hokka, D., Jimbo, N., et al. (2020). A novel EWSR1-VGLL1 gene fusion in a soft tissue malignant myoepithelial tumor. Genes Chromosomes Cancer *59*, 249–254.
20. Im, J.Y., Kim, D.M., Park, H., Kang, M.J., Kim, D.Y., Chang, K.Y., Kim, B.K., and Won, M. (2021). VGLL1 phosphorylation and activation promotes gastric cancer malignancy via TGF-beta/ERK/RSK2 signaling. Biochim. Biophys. Acta. Mol. Cell Res. *1868*, 118892.
21. Castilla, M.Á., López-García, M.Á., Atienza, M.R., Rosa-Rosa, J.M., Díaz-Martín, J., Pecero, M.L., Vieites, B., Romero-Pérez, L., Benítez, J., Calcabrini, A., and Palacios, J. (2014). VGLL1 expression is associated with a triple-negative basal-like phenotype in breast cancer. Endocr. Relat. Cancer *21*, 587–599.
22. Chang, G., Shi, L., Ye, Y., Shi, H., Zeng, L., Tiwary, S., Huse, J.T., Huo, L., Ma, L., Ma, Y., et al. (2020). YTHDF3 Induces the Translation of m(6)A-Enriched Gene Transcripts to Promote Breast Cancer Brain Metastasis. Cancer Cell *38*, 857–871.e7.
23. Liu, T., Wei, Q., Jin, J., Luo, Q., Liu, Y., Yang, Y., Cheng, C., Li, L., Pi, J., Si, Y., et al. (2020). The m6A reader YTHDF1 promotes ovarian cancer progression via augmenting EIF3C translation. Nucleic Acids Res. *48*, 3816–3831.
24. Liao, S., Sun, H., and Xu, C. (2018). YTH Domain: A Family of N(6)-methyladenosine (m(6)A) Readers. Dev. Reprod. Biol. *16*, 99–107.
25. Zheng, G., Dahl, J.A., Niu, Y., Fedorcsak, P., Huang, C.M., Li, C.J., Vågbø, C.B., Shi, Y., Wang, W.L., Song, S.H., et al. (2013). ALKBH5 is a mammalian RNA demethylase that impacts RNA metabolism and mouse fertility. Mol. Cell *49*, 18–29.
26. Liu, Z., Wang, T., She, Y., Wu, K., Gu, S., Li, L., Dong, C., Chen, C., and Zhou, Y. (2021). N(6)-methyladenosine-modified circIGF2BP3 inhibits CD8(+) T-cell responses to facilitate tumor immune evasion by promoting the deubiquitination of PD-L1 in non-small cell lung cancer. Mol. Cancer *20*, 105.
27. Chen, H., Gao, S., Liu, W., Wong, C.C., Wu, J., Wu, J., Liu, D., Gou, H., Kang, W., Zhai, J., et al. (2021). RNA N(6)-Methyladenosine Methyltransferase METTL3 Facilitates Colorectal Cancer by Activating the m(6)A-GLUT1-mTORC1 Axis and Is a Therapeutic Target. Gastroenterology *160*, 1284–1300.e16.
28. Li, C., Tang, Z., Zhang, W., Ye, Z., and Liu, F. (2021). GEPIA2021: integrating multiple deconvolution-based analysis into GEPIA. Nucleic Acids Res. *49*, W242–W246.
29. Keenan, A.B., Torre, D., Lachmann, A., Leong, A.K., Wojciechowicz, M.L., Utti, V., Jagodnik, K.M., Kropiwnicki, E., Wang, Z., and Ma'ayan, A. (2019). ChEA3: transcription factor enrichment analysis by orthogonal omics integration. Nucleic Acids Res. *47*, W212–W224.
30. Zhang, Q., Liu, W., Zhang, H.M., Xie, G.Y., Miao, Y.R., Xia, M., and Guo, A.Y. (2020). hTFtarget: A Comprehensive Database for Regulations of Human Transcription Factors and Their Targets. Dev. Reprod. Biol. *18*, 120–128.

31. Osman, I., He, X., Liu, J., Dong, K., Wen, T., Zhang, F., Yu, L., Hu, G., Xin, H., Zhang, W., and Zhou, J. (2019). TEAD1 (TEA Domain Transcription Factor 1) Promotes Smooth Muscle Cell Proliferation Through Upregulating SLC1A5 (Solute Carrier Family 1 Member 5)-Mediated Glutamine Uptake. Circ. Res. *124*, 1309–1322.
32. Resar, L., Chia, L., and Xian, L. (2018). Lessons from the Crypt: HMGA1-Amping up Wnt for Stem Cells and Tumor Progression. Cancer Res. *78*, 1890–1897.
33. Zhang, H., Duan, H.L., Wang, S., Liu, Y., Ding, G.N., and Lin, R.X. (2022). Epigenetic signature associated with thyroid cancer progression and metastasis. Semin. Cancer Biol. *83*, 261–268.
34. Yue, Y., Liu, J., and He, C. (2015). RNA N6-methyladenosine methylation in post-transcriptional gene expression regulation. Genes Dev. *29*, 1343–1355.
35. Zhou, Y., Zeng, P., Li, Y.H., Zhang, Z., and Cui, Q. (2016). SRAMP: prediction of mammalian N6-methyladenosine (m6A) sites based on sequence-derived features. Nucleic Acids Res. *44*, e91.
36. Yin, M., Li, X., Tan, S., Zhou, H.J., Ji, W., Bellone, S., Xu, X., Zhang, H., Santin, A.D., Lou, G., and Min, W. (2016). Tumor-associated macrophages drive spheroid formation during early transcoelomic metastasis of ovarian cancer. J. Clin. Invest. *126*, 4157–4173.
37. Hanahan, D., and Weinberg, R.A. (2011). Hallmarks of cancer: the next generation. Cell *144*, 646–674.
38. Kalluri, R., and Weinberg, R.A. (2009). The basics of epithelial-mesenchymal transition. J. Clin. Invest. *119*, 1420–1428.
39. Pegoraro, S., Ros, G., Piazza, S., Sommaggio, R., Ciani, Y., Rosato, A., Sgarra, R., Del Sal, G., and Manfioletti, G. (2013). HMGA1 promotes metastatic processes in basal-like breast cancer regulating EMT and stemness. Oncotarget *4*, 1293–1308.
40. Belton, A., Gabrovsky, A., Bae, Y.K., Reeves, R., Iacobuzio-Donahue, C., Huso, D.L., and Resar, L.M.S. (2012). HMGA1 induces intestinal polyposis in transgenic mice and drives tumor progression and stem cell properties in colon cancer cells. PLoS One *7*, e30034.
41. Han, X., Cao, Y., Wang, K., and Zhu, G. (2016). HMGA1 facilitates tumor progression through regulating Wnt/beta-catenin pathway in endometrial cancer. Biomed. Pharmacother. *82*, 312–318.
42. McMellen, A., Woodruff, E.R., Corr, B.R., Bitler, B.G., and Moroney, M.R. (2020). Wnt Signaling in Gynecologic Malignancies. Int. J. Mol. Sci. *21*, 4272.
43. Hiremath, I.S., Goel, A., Warrier, S., Kumar, A.P., Sethi, G., and Garg, M. (2022). The multidimensional role of the Wnt/beta-catenin signaling pathway in human malignancies. J. Cell. Physiol. *237*, 199–238.
44. Soncin, F., Khater, M., To, C., Pizzo, D., Farah, O., Wakeland, A., Arul Nambi Rajan, K., Nelson, K.K., Chang, C.W., Moretto-Zita, M., et al. (2018). Comparative analysis of mouse and human placentae across gestation reveals species-specific regulators of placental development. Development *145*, dev156273.
45. Pobbati, A.V., Chan, S.W., Lee, I., Song, H., and Hong, W. (2012). Structural and functional similarity between the Vgll1-TEAD and the YAP-TEAD complexes. Structure *20*, 1135–1140.
46. Ma, S., Chen, C., Ji, X., Liu, J., Zhou, Q., Wang, G., Yuan, W., Kan, Q., and Sun, Z. (2019). The interplay between m6A RNA methylation and noncoding RNA in cancer. J. Hematol. Oncol. *12*, 121.
47. Huang, G.W., Chen, Q.Q., Ma, C.C., Xie, L.H., and Gu, J. (2021). linc01305 promotes metastasis and proliferation of esophageal squamous cell carcinoma through interacting with IGF2BP2 and IGF2BP3 to stabilize HTR3A mRNA. Int. J. Biochem. Cell Biol. *136*, 106015.
48. Li, H., Zhang, W., Yan, M., Qiu, J., Chen, J., Sun, X., Chen, X., Song, L., and Zhang, Y. (2019). Nucleolar and spindle associated protein 1 promotes metastasis of cervical carcinoma cells by activating Wnt/beta-catenin signaling. J. Exp. Clin. Cancer Res. *38*, 33.
49. Zhang, S., Xu, Y., Xie, C., Ren, L., Wu, G., Yang, M., Wu, X., Tang, M., Hu, Y., Li, Z., et al. (2021). RNF219/alpha-Catenin/LGALS3 Axis Promotes Hepatocellular Carcinoma Bone Metastasis and Associated Skeletal Complications. Adv. Sci. *8*, 2001961.
50. Li, H., Zhang, W., Niu, C., Lin, C., Wu, X., Jian, Y., Li, Y., Ye, L., Dai, Y., Ouyang, Y., et al. (2019). Nuclear orphan receptor NR2F6 confers cisplatin resistance in epithelial ovarian cancer cells by activating the Notch3 signaling pathway. Int. J. Cancer *145*, 1921–1934.

STAR★METHODS

KEY RESOURCES TABLE

REAGENT or RESOURCE	SOURCE	IDENTIFIER
Antibodies		
Rabbit polyclonal anti- VGLL1	Proteintech	Cat No: 10124-2-AP; RRID: AB_2218174
Rabbit polyclonal anti-β-catenin	Proteintech	Cat No: 51067-2-AP; RRID:AB_2086128
Rabbit monoclonal anti-HMGA1	Cell Signaling Technology	Cat#12094S
Rabbit polyclonal anti-METTL3	Proteintech	Cat No: 15073-1-AP; RRID:AB_2142033
Mouse monoclonal anti-IGF2BP2	Abcam	Cat No: Ab128175; RRID:AB_11150982
Rabbit monoclonal anti-GAPDH	Cell Signaling Technology	Cat#5174S
Rabbit monoclonal anti-α-tubulin	Cell Signaling Technology	Cat No: #2125S
Rabbit monoclonal anti-Flag	Cell Signaling Technology	Cat No: #14793S
Mouse monoclonal anti-P84	Abcam	Cat No: Ab487; RRID:AB_304696
Mouse monoclonal anti-E-cadherin	Cell Signaling Technology	Cat No:14472S
Rabbit monoclonal anti-N-cadherin	Cell Signaling Technology	Cat No:13116S
Rabbit monoclonal anti-Vimentin	Cell Signaling Technology	Cat No:46173S
Mouse monoclonal anti-RNA polymerase II	Sigma–Aldrich	Cat No: 04-1570-I; RRID:AB_2801298
Mouse monoclonal anti-P300	Abcam	Cat No: Ab14984; RRID:AB_301550
Rabbit monoclonal anti- H3K4me3	Cell Signaling Technology	Cat No: #9751S
Mouse monoclonal anti-TEAD4	Abcam	Cat No: Ab58310; RRID:AB_945789
Mouse monoclonal anti-MYC	Cell Signaling Technology	Cat No: #2276S
Rabbit monoclonal anti-SLUG	Cell Signaling Technology	Cat No:9585S
Rabbit polyclonal anti- SNAIL	Proteintech	Cat No:13099-1-AP; RRID:AB_2191756
Chemicals, peptides, and recombinant proteins		
XAV-939	Selleck	Cat No: S1180
Triton X-100	Beyotime	Cat No: ST795
Flag affinity agarose	Sigma–Aldrich	Cat No: A4596
MYC affinity agarose	Sigma–Aldrich	Cat No: A7470
Glycine	Sangon Biotech	Cat No: A502065
ECL reagent	Millipore	Cat No: WBKLS0500
TRIzol reagent	Invitrogen	Cat No: #15596018
Lipofectamine 3000 Transfection Reagent	Invitrogen	Cat No: L3000008
Tween 20	Beyotime	Cat No: #ST825-100mL
Crystal violet	Sigma-Aldrich	Cat No: #V5265
Protein A/G Agarose Beads	Santa Cruz	Cat No: sc-2003
TBS	Beyotime	Cat No: #P0228
Non-fat milk	Beyotime	Cat No: P0216
DMSO	Sangon Biotech	Cat No: A503039
2-(4-Amidinophenyl)-6-indolecarbamidine dihydrochloride (DAPI)	Beyotime	Cat No: C1002
Critical commercial assays		
Color Reverse Transcription Kit	EZBioscience	Cat No: A0010CGQ
Magna RIP RNA-Binding Protein Immunoprecipitation Kit	Millipore	Cat No: 17–700
MTT assay kit	Sangon Biotech	Cat No: E606334

(*Continued on next page*)

Continued

REAGENT or RESOURCE	SOURCE	IDENTIFIER
Dual Luciferase Reporter Assay Kit	Promega	Cat No: E1910
5-Ethynyl-2-deoxyuridine (EdU) labeling/detection kit	Ribobio	Cat No: C10310
SYBR Green PCR kit	Roche	Cat No: #QR0100
Deposited data		
Raw and analyzed data	This paper	PRJNA1056280, PRJNA1056471
Experimental models: Cell lines		
Human: OVCAR3	ATCC	HTB-161
Human: SKOV3	ATCC	HTB-77
Human: TOV112D	ATCC	CRL-3593
Human: CAOV3	ATCC	HTB-75
Human: COV362	CoBioER	CBP60835
Human: OVCAR4	CoBioER	CBP60556
Human: COV644	ChuanQiu Biotechnology	N/A
Human: A2780	Procell Life Science & Technology	CL-0013
Human: OV90	Procell Life Science & Technology	CL-0626
Human: HosePic	Jennio Biotech	N/A
Human: FT282	Jennio Biotech	CRL-3449
Experimental models: Organisms/strains		
BALB/c-nude mice (female, 4–5 weeks old)	Beijing SiPeiFu	N/A
Oligonucleotides		
shRNA targeting sequence 1: VGLL1: 5′- GGTGATGGTCCAGAATTAAGA-3′	Jiangsu Saisofi Biotechnology Co., Ltd (wuxi, China)	N/A
shRNA targeting sequence 2: VGLL1: 5′- GCCAGTACCAGCCTTCCAAAT-3′	Jiangsu Saisofi Biotechnology Co., Ltd (wuxi, China)	N/A
shRNA targeting sequence: HMGA1: 5′- CCAGCGAAGTGCCAACACCTA-3′	Jiangsu Saisofi Biotechnology Co., Ltd (wuxi, China)	N/A
shRNA targeting sequence: IGF2BP2: 5′-CAGTGCTGAGATAGAGATTAT-3′	Jiangsu Saisofi Biotechnology Co., Ltd (wuxi, China)	N/A
siRNA targeting sequence 1: HMGA1: 5′-AGCCGGTGCTGCGCTCCTCTAAT-3′	RiboBio (Guangzhou, China)	N/A
siRNA targeting sequence 1: METTL3 5′-CCGCGTGAGAATTGGCTATATCC-3′	RiboBio (Guangzhou, China)	N/A
siRNA targeting sequence 1: IGF2BP2: 5′-CGCGGGCTCTCGGGGAAGAGACG-3′	RiboBio (Guangzhou, China)	N/A
Primers for ChIP assays, see Table S4	This paper	N/A
Primers for qRT-PCR, see Table S5	This paper	N/A
Recombinant DNA		
Plasmid: pSLenti-SFH-EGFP-P2A-Puro-CMV vector	Jiangsu Saisofi Biotechnology Co., Ltd (wuxi, China)	N/A
Plasmid: pLVX-*retro*-hygro vector	Jiangsu Saisofi Biotechnology Co., Ltd (wuxi, China)	N/A
Plasmid: pSuper-*retro*-puro vector	Jiangsu Saisofi Biotechnology Co., Ltd (wuxi, China)	N/A
Software and algorithms		
Carl Zeiss AxioVision Rel. 4.6	Carl Zeiss Microscopy GmbH	https://carl-zeiss-axiovision-rel.software.informer.com/4.6/
GraphPad Prism 8.0	GraphPad Software	https://www.graphpad.com/
SPSS 22.0	SPSS	https://www.graphpad.com/

RESOURCE AVAILABILITY

Lead contact

Further information and requests for resources and reagents should be directed to and will be fulfilled by the lead contact, Jianchuan Xia (xiajch@mail.sysu.edu.cn).

Materials availability

All materials used in this study are either commercially available or through collaboration, as indicated.

Data and code availability

- The RNA-seq data can be found at the following SRA accession number: PRJNA1056280, PRJNA1056471. And the dataset is publicly accessible.
- This paper does not report original code.
- Any additional information required to reanalyze the data reported in this paper is available from the lead contact upon request.

EXPERIMENTAL MODEL AND STUDY PARTICIPANT DETAILS

Cell lines and cell culture

The human OC cell lines OVCAR3, SKOV3, TOV112D and CAOV3 were obtained from the American Type Culture Collection (Manassas, VA, USA). A2780 and OV90 cells were purchased from Procell Life Science & Technology Co., Ltd. (Wuhan, China). COV362 and OVCAR4 were obtained from CoBioER (Nanjing, China). COV644 cells were purchased from ChuanQiu Biotechnology (Shanghai, China). HosePic and FT282 cells were obtained from Jennio Biotech Co., Ltd. (Guangzhou, China). All these cells were authenticated using short tandem repeat profiling. All the cell lines were grown in Dulbecco's modified Eagle's medium (DMEM) (Gibco, Grand Island, NY) supplemented with 20% fetal bovine serum (Gibco, Grand Island, NY) according to the manufacturer's instructions. Additionally, OVCAR-3 were cultured in RPMI1640 with 20% fetal bovine serum.

Xenograft tumor models

BALB/c-nude mice (female, 4–5 weeks old) were purchased and housed in barrier facilities on a 12 h light/dark cycle. In the tumor model, the indicated luciferase-expressing cells (1×10^6 OVCAR3-sh NC, OVCAR3-shVGLL1#1, or OVCAR3-sh VGLL1#1/VGLL1 cells) were stereotactically implanted into the ovary of nude mice. Tumors were detected using a Xenogen IVIS imaging system. At the experimental endpoint, the animals were euthanized, and the tumors were excised, weighed, paraffin-embedded and sectioned for immunohistochemistry and hematoxylin–eosin (H&E) staining. Images were captured using the AxioVision Rel. 4.6 computerized image analysis system (Carl Zeiss, Oberkochen, Germany).

In the *in vivo* target VGLL1 therapy efficiency test, mice were randomly divided into two groups (n = 6 per group). After 10 days of injection of 1×10^6 OVCAR3-shVGLL1#1^{Dox} cells, one group of mice was administered Dox (2 mg/mL) in drinking water to induce VGLL1 downregulation in the tumors. Tumors were examined every 3 days. After 6 weeks of injection, animals were euthanized, and tumors were excised and weighed. Tumors were detected using a Xenogen IVIS imaging system.

The Institutional Animal Care and Use Committee of Sun Yat-sen University approved the experimental procedures. The study ethical approval number for the mouse study was L102012020120V.

Patient specimens

Cancer samples were obtained from the Sun Yat-sen University Cancer Center for this study. Ovarian cancer samples and normal ovary samples were collected from women patients from the Han Chinese, and they are East Asian ancestry. Seventy-two normal ovary tissues were collected from these patients: benign postmenopausal patients with uterine fibroids who requested hysterectomy and ovariectomy. We collected normal ovarian tissue from these patients. Among these seventy-two normal ovary tissues, 13 cases were used for both IHC analysis and qPCR analysis; And 59 cases were used for qPCR analysis only (The study protocols were approved by the Institutional Research Ethics Committee of Sun Yat-sen University Cancer Center. The ethical study approval number: SL-B2021-396-01). Table S1 summarizes the clinicopathological characteristics of 157 formalin-fixed, paraffin-embedded (FFPE) ovarian cancer samples. These characteristics include gender, age, FIGO stage, histological type, intraperitoneal metastasis classification, intestinal metastasis classification, expression of VGLL1, tumor recurrence, ascites with tumor cells status and patient survival status. All the 157 ovarian cancer patients were female (100%), including 53.3% aged $\leq$53 and 46.5% aged>53. No association was found between the gender or the age and VGLL1 expression in the specimens in this study. Among these 157 OC tissues, 126 cases had both RNA and paraffin-embedded tissue and were tested for both IHC and qPCR analysis, while the remaining 31 cases had only paraffin-embedded tissue and were tested for IHC only. Additionally, among these 157 OC tissues, 76 primary OC tissues and its paired metastatic nodules used for qPCR; In addition, 22 cases of the above paired metastatic nodules were also used for IHC analysis. Ten fresh OC tissues (five primary OC tissues and five paired metastatic OC nodules) were collected, and RNA extraction and RNA-seq analysis were performed on them.

The study protocols were approved by the Institutional Research Ethics Committee of Sun Yat-sen University Cancer Center for the use of these clinical materials for research purposes (The ethical study approval number: SL-B2021-396-01). Each patient signed a written informed consent for all the procedures.

METHOD DETAILS

RNA isolation, reverse transcription and qRT–PCR

Total RNA from cells was extracted using TRIzol reagent (Invitrogen, Carlsbad, CA) according to the manufacturer's protocol. The retrieved RNA was reverse-transcribed using a Color Reverse Transcription Kit (EZBioscience) and amplified on a CFX96 Real-Time System (Bio-Rad Laboratories, Singapore). The relative expression levels were normalized to GAPDH and calculated as $2^{-[(Ct\ of\ gene)-(Ct\ of\ GAPDH)]}$, in which Ct represents the cycle threshold for each transcript. The primers used in qRT–PCR are listed in Table S5.

RNA sequencing

We extracted total RNA from five samples of nonmetastatic OC and five samples of metastatic OC using TRIzol reagent (Invitrogen, Carlsbad, CA, USA) and further purified the extracted RNA using rRNA depletion. cDNA was synthesized from the RNA, followed by PCR amplification. We then constructed RNA-seq libraries, which were sequenced on the Illumina HiSeq2500 platform (Illumina, San Diego, CA, USA).

Wound healing assay

The cells were seeded in six-well plates (Nest, Biotechnology, Jiangsu, China) with DMEM containing 10% FBS overnight. The cell monolayers were wounded by scratching with sterile plastic 10-μL micropipette tips to create artificial wounds and rinsed 2 times with PBS. Subsequently, the cells were cultured for 48 h. Images of the different stages of wound healing were photographed via an inverted Olympus IX50 microscope with a 10× objective lens at 0, 24 and 48 h.

mRNA stability assay

Briefly, mRNA stability assay was performed as follows. Cells were treated with Actinomycin D (5 μg/mL) for various time, followed by total RNA isolation. The total RNAs were used for cDNA synthesis, followed by PCR amplification with actin and VGLL1 primers. The relative percentage of remaining VGLL1 RNA was calculated by normalizing VGLL1 mRNA from triplicate samples (mean ± SD) and then plotted to calculate the half-life of VGLL1 mRNA.

Protein immunoprecipitation (IP) assays

Lysates were prepared from A2780 cells using lysis buffer (150 mM NaCl, 10 mM HEPES, pH 7.4, 1% NP-40). Lysates were incubated with Flag affinity agarose (Sigma–Aldrich), MYC affinity agarose (Sigma–Aldrich), Flag antibody (#14793; Cell Signaling Technology), or MYC antibody (#2276; Cell Signaling Technology) with protein G agarose overnight at 4°C. Beads containing affinity-bound proteins were washed six times using immunoprecipitation wash buffer (150 mM NaCl, 10 mM HEPES, pH 7.4, 0.1% NP-40); lysates were eluted using 1 M glycine (pH 3.0). The eluates were then mixed with sample buffer, denatured, and used for western blot analysis.

RNA immunoprecipitation (RIP) assays

RIP assays were performed according to the manufacturer's instructions (the Magna RIP RNA-Binding Protein Immunoprecipitation Kit,17–700, Millipore) to detect interactions between the proteins and mRNAs in ovarian cancer cells. Briefly, magnetic beads coated with 5 μg of specific antibodies against mouse immunoglobulin G (17–700, Millipore), or IGF2BP2 (ab#128175, Abcam) were incubated with prepared cell lysates (from 2.0×10^7 cells) overnight at 4°C. Then, the RNA-protein complexes were washed 6 times and incubated with proteinase K digestion buffer. RNA (nearly 40ug) was finally extracted by phenol-chloroform RNA extraction methods. The relative interaction between IGF2BP2 and VGLL1 transcripts was determined by RT-PCR analysis and Agarose electrophoresis assay in OC cells, normalized to the input. Additionally, the retrieved pellets were then subjected to qRT–PCR analysis using the qRT–PCR primers for VGLL1. GAPDH was used as a negative control. Primers are provided in Table S5.

Immunohistochemistry (IHC)

IHC was performed on formalin-fixed, paraffin-embedded human tissue sections as described before.[48] IHC analysis was performed to determine altered protein expression in paraffin-embedded ovarian cancer tissues and peritoneal metastasis tissues with anti-VGLL1 (Proteintech, 10124-2-AP), anti-β-catenin (Proteintech, 51067-2-AP), anti-HMGA1 (Active Motif, 39615), anti-METTL3 (Proteintech, 15073-1-AP), and antibodies overnight at 4°C. The degree of immunostaining of formalin-fixed, paraffin-embedded sections was reviewed and scored separately by two independent pathologists blinded to the histopathological features and patient data of the samples. The scores were determined by combining the proportion of positively stained tumor cells and the intensity of staining. The scores given by the two independent pathologists were combined into a mean score for further comparative evaluation. Tumor cell proportions were scored as follows: 0, no positive tumor cells; 1, <10% positive tumor cells; 2, 10%–35% positive tumor cells; 3, 35%–75% positive tumor cells; 4, >75% positive tumor cells. Staining intensity was graded according to the following standard: 0, no staining; 1, weak staining (light yellow); 2, moderate staining

(yellow brown); 3, strong staining (brown). The staining index (SI) was calculated as the product of the staining intensity score and the proportion of positive tumor cells. Using this method of assessment, we evaluated protein expression in normal breast tissues, breast tumor tissues and bone metastasis tissues by determining the SI, with possible scores of 0, 1, 2, 3, 4, 6, 8, 9 and 12. Samples with an SI $\geq$ 6 were determined to have high expression, and samples with an SI < 6 were determined to have low expression.

Mean optical density (MOD) analysis

IHC staining for protein expression of VGLL1 in OC samples with or without metastasis was quantitatively analyzed by using the AxioVision 4.6 computerized image analysis system assisted with an automatic measurement program (Carl Zeiss). The method of mean optical density (MOD) was used to determine the immunostaining intensity of each tested specimen. Briefly, the stained sections were evaluated at ×200 magnification, and 10 representative staining fields of each section were analyzed to verify the MOD, which represents the strength of staining signals as measured per positive pixel, according to a previously reported study.[49] The MOD data were statistically analyzed by using the t test to compare the average MOD difference between different groups of tissues, and $p < 0.05$ was regarded as significant.

Western blot analysis

Western blot analyses were performed[50] using primary antibodies, including anti-VGLL1 (Proteintech, 10124-2-AP), anti-β-catenin (Proteintech, 51067-2-AP), anti-HMGA1 (Active Motif, 39615), and anti-METTL3 (Proteintech, 15073-1-AP). The membranes were stripped and re-incubated with anti-α-Tubulin as a loading control. P84 (Abcam, ab487) was used as a nuclear marker.

Transwell matrix invasion assay

Cells (1×10^4) suspended in the upper chamber of polycarbonate Transwell filters coated with Matrigel (BD Biosciences, San Jose, CA, USA) were cultured at 37°C for 24 h. Then, the cells inside the upper chamber were removed with cotton swabs, and the cells that had migrated to the bottom surface of the membrane where 10% FBS was added as an attractant were fixed in 1% paraformaldehyde, stained with crystal violet and counted in five random fields of view per well. The data are shown as the mean ± SD.

Immunofluorescence

Cells (5×10^4) were plated on coverslips. The cells were washed three times with PBS and treated with PBS containing 1% Triton X-100. Next, the cells were stained with a primary anti-β-Catenin antibody (Cell Signaling Technology, #8480, 1:100) or anti- E-cadherin antibody (Cell Signaling Technology, #14472, 1:200) or anti- Vimentin antibody (Cell Signaling Technology, #46173, 1:100) for 2 h at 4°C according to the manufacturer's instructions. For the colonization staining of TEAD4 and VGLL1, cells were washed three times with PBS, treated with PBS containing 1% Triton X-100 and then stained with anti-TEAD4 (Novus Biologicals, NBP1-32765, 1:200) and anti-VGLL1 antibodies (Proteintech, 10124-2-AP, 1:200). After washing three times with PBS, the cells were incubated with rhodamine-conjugated goat anti-rabbit or anti-mouse antibody (Cell Signaling Technology, 1:100) at 37°C for 1 h. Cells were counterstained with DAPI (Sigma–Aldrich) to visualize the nuclei. The percentage of membrane colonization of TEAD4 and VGLL1 was counted in five random fields.

Cell proliferation assays

MTT assays were performed according to the protocol of the MTT assay kit (Sangon Biotech Co., Ltd.). Briefly, cells were seeded into 96-well plates at a density of 2×10^3 cells/well. Cell viability was assessed using the MTT assay kit at 24, 48, 72, and 96 h according to the manufacturer's protocol. After 4 h of incubation in MTT reagent at 37°C and 5% CO_2, the medium was replaced with 150 μL dimethyl sulfoxide at room temperature (DMSO; Sangon Biotech Co., Ltd.). The absorbance of each sample was measured at 450 nm using a microplate spectrophotometer (BioTek Instruments, Inc.).

EdU assays were conducted according to the protocol of the 5-Ethynyl-2-deoxyuridine (EdU) labeling/detection kit (Ribobio, Guangzhou, China). Briefly, the cells were seeded in 24-well plates containing sterile glass coverslips at 37°C overnight. Then, the images were visualized by a fluorescence microscope.

TOP/FOP flash activity assays

The wild-type (TOP) and mutant (FOP) LEF/TCF reporters were cloned into pGL3 luciferase constructs (Promega). Twenty thousand cells were seeded in triplicate in 48-well plates and allowed to settle for 24 h. One hundred nanograms of TOP or FOP flash, plus 1 ng of pRLTK Renilla plasmid (Promega), was transfected into cells using the Lipofectamine 3000 reagent according to the manufacturer's recommendation. Luciferase and Renilla signals were measured 24 h after transfection using the Dual Luciferase Reporter Assay Kit (Promega) according to a protocol provided by the manufacturer. The results were calculated as the ratio of specific TOP-Flash to nonspecific FOP-Flash relative Renilla luciferase units (RLU).

Methylated RNA immunoprecipitation (MeRIP)

RNA immunoprecipitation was performed with Protein A/G Agarose Beads (Santa Cruz) following the manufacturer's instructions. Briefly, Protein A/G Agarose Beads coated with 5 mg of normal antibodies against rabbit immunoglobulin G (Beyotime), Ago2 (Abcam, Ab186733), or m^6A (Abcam, Ab286164) were incubated with prefrozen cell lysates or nuclear extracts overnight at 4°C. Associated RNA–protein complexes

were collected and washed 6 times and then subjected to proteinase K digestion and RNA extraction by TRIzol. The relative interaction between protein and RNA was determined by qRT−PCR and PCR and normalized to the input. Primers are provided in Table S4.

Luciferase activity assay

Cells (1×10^4) were seeded in 48-well plates in triplicate and allowed to proliferate to 60–80% confluence after 24 h in culture. The indicated plasmids or luciferase reporter plasmids plus 1 ng of pRL-TK Renilla plasmid (Promega, Madison, WI) were transfected into cells using Lipofectamine 3000 reagent (Invitrogen) according to the manufacturer's instructions. Luciferase and Renilla enzyme activity signals were measured using the Dual Luciferase Reporter Assay Kit (Promega) following the manufacturer's protocol.

DNA constructs and establishment of stable cell lines

The human VGLL1 and TEAD4 coding sequence was amplified by the polymerase chain reaction and subcloning into a the pSLenti-SFH-EGFP-P2A-Puro-CMV vector and pLVX-*retro*-hygro vector. To re-express VGLL1 in sh VGLL1#1 cells (cells treated with a short hairpin RNA (shRNA) targeting VGLL1), the VGLL1-expressing construct was edited with the same sense mutations to prevent sh VGLL1#1-mediated downregulation. To silence endogenous VGLL1, short hairpin RNA (shRNA) oligonucleotides were cloned into the pSuper-*retro*-puro vector. The targeting sequences of shRNAs are provided in Table S4. Stable cells were generated from cell pools by lentivirus or retroviral infection using pSLenti-SFH-EGFP-P2A-Puro-CMV for VGLL1 overexpression and p-Super-*retro*-puro for silencing of VGLL1. Briefly, lentivirus or retroviral vectors were co-transfected with packaging plasmids into 293T cells. The supernatant containing the virus was collected, and viral infections were performed serially for 3 days. Stable cell lines were selected with 1.0 μg/mL puromycin, 25 μg/mL hygromycin, respectively.

Chromatin immunoprecipitation (ChIP) assay

ChIP assays were performed as previously described.[50] The indicated cells (4×10^6) in a 100-mm culture dish were treated with a 1% final concentration of formaldehyde to cross-link proteins to DNA, and the reaction was stopped by the addition of glycine. The cell lysates were sonicated to shear the DNA to fragments of 300–1,000 bp. Chromatin supernatants were incubated with anti-H3K4me3 (#9751; Cell Signaling Technology), anti-TEAD4 (#ab58310; Abcam), anti-Flag (#14793; Cell Signaling Technology), anti-p300 (#ab14984; Abcam), anti-RNA polymerase II (#05–623; Millipore), or anti-immunoglobulin G antibody (#I8765; Sigma–Aldrich) overnight at 4°C with rotation. After reversing the cross-linking of protein/DNA complexes to free DNA, PCR was performed using the primers listed in Table S4.

QUANTIFICATION AND STATISTICAL ANALYSIS

SPSS version 22.0 (IBM Corp., Armonk, NY) was used for all statistical analyses. All experiments were performed with at least three replicates, and data were expressed as mean G standard deviation. The ANOVA test, Two-sided χ^2 test, Fisher's exact test, log rank test, Spearman-rank correlation test, and Student's *t* test were used for data analysis. Clinical data were analyzed by Fisher's exact test. Kaplan-Meier method was used to calculate the survival rate and Log rank test for the different significance. Correlation between the expression of genes was calculated using Pearson correlation. Correlation analyses between VGLL1 expression and patient status or metastasis status was calculated by Two-sided χ^2 test. A Cox regression model was used for multivariate statistical analysis. Student's t tests were used for comparing two variables. The ANOVA test was used for multiple variables comparison. Statistical significance of the differences was considered at $p < 0.05$. The meaning of asterisks number was *$p < 0.05$, **$p < 0.01$, ***$p < 0.001$, and ns means not significant.